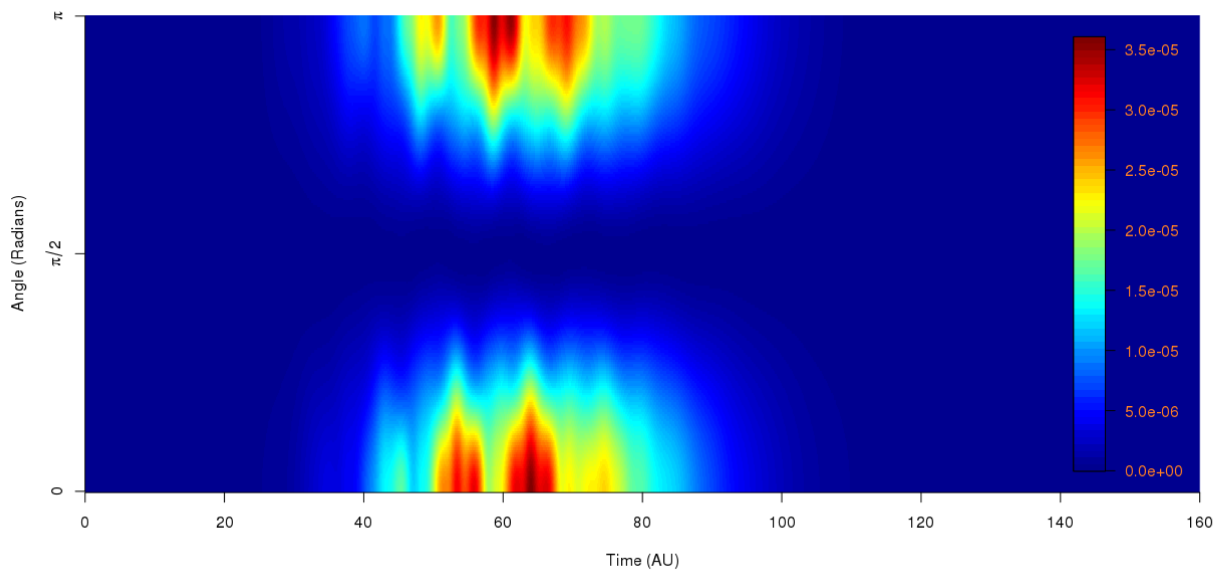


**IOP** | Institute of Physics  
**Computational Physics Group**Newsletter

---

---

Angle dependent radial current density at a fixed radius as a function of time

**A New GPU-based Computational Framework for the Ab-initio Solution of the TDSE for Atomic and Molecular One-Electron Systems under Intense Ultra-Short Laser Fields**

(image courtesy of Dr Cathal Ó Broin)

---

# Newsletter Contents

<b>This Newsletter...</b>	<b>3</b>
<b>A New GPU-based Computational Framework for the Ab-initio Solution of the TDSE for Atomic and Molecular One-Electron Systems under Intense Ultra-Short Laser Fields</b>	<b>4</b>
Introduction . . . . .	4
RMT Theory for Molecules . . . . .	4
CLTDSE . . . . .	6
GPGPU . . . . .	7
Concluding statement . . . . .	9
Acknowledgment . . . . .	10
<b>Tensor Networks and Geometry for the Modelling of Disordered Quantum Many-Body Systems</b>	<b>11</b>
Introduction . . . . .	11
Matrix Product States . . . . .	12
Tensor networks . . . . .	14
The Area Law for Entanglement Entropy . . . . .	14
Beyond the Area Law . . . . .	14
Structurally Inhomogeneous tensor networks . . . . .	15
Correlation Functions . . . . .	16
Entanglement Entropy . . . . .	17
Conclusion and Outlook . . . . .	18
<b>Hydrogen and helium under extreme pressures</b>	<b>21</b>
Introduction . . . . .	21
Phase diagram . . . . .	21
High pressure hydrogen . . . . .	23
High pressure helium . . . . .	23
Outlook . . . . .	25
Acknowledgment . . . . .	26
<b>Computational Physics Group News</b>	<b>28</b>
The Computational Physics Annual PhD Thesis Prize . . . . .	28
IoP Computational Physics Group - Research Student Conference Fund . . . . .	29
<b>Conference and Workshop reports</b>	<b>29</b>
47 <sup>th</sup> Annual APS-DAMOP Meeting Providence (RI),USA ,2016. . . . .	29
American Physical Society (APS),USA,2016. . . . .	30
<b>Upcoming Events of Interest</b>	<b>31</b>
<b>Computational Physics Group Committee</b>	<b>31</b>
<b>Related Newsletters and Useful Websites</b>	<b>32</b>

# This Newsletter...

Dear Readers,

The feature article for this bumper edition of the newsletter is an invited contribution by Dr Cathal Ó Broin from the Dublin City University, our winner of the 2016 IoP Computational Physics Group PhD Prize, on *'A New GPU-based Computational Framework for the Ab-initio Solution of the TDSE for Atomic and Molecular One-Electron Systems under Intense Ultra-Short Laser Fields'*.

Dr Cathal Ó Broin also kindly provided the cover image for this edition.

In addition, we have two invited contributions from Bartomeu Monserrat and Andrew Goldsborough our runners-up of the 2014 and of the 2016 IoP Computational Physics Group PhD Prize.

Most URLs in the newsletter have web hyperlinks and clicking on them should take you to the corresponding page. The current edition of the newsletter can be found online at:

[www.iop.org/activity/groups/subject/comp/news/page\\_40572.html](http://www.iop.org/activity/groups/subject/comp/news/page_40572.html)

with previous editions at:

[www.iop.org/activity/groups/subject/comp/news/archive/page\\_53142.html](http://www.iop.org/activity/groups/subject/comp/news/archive/page_53142.html)

[www.soton.ac.uk/~fangohr/iop\\_cpg.html](http://www.soton.ac.uk/~fangohr/iop_cpg.html)

As always, we value your feedback and suggestions. Enjoy this edition!

*Marco Pinna, Newsletter Editor* ✉ [mpinna@lincoln.ac.uk](mailto:mpinna@lincoln.ac.uk))

(on behalf of the The Computational Physics Group Committee).

# A New GPU-based Computational Framework for the Ab-initio Solution of the TDSE for Atomic and Molecular One-Electron Systems under Intense Ultra-Short Laser Fields

Cathal Ó Broin

Irish Centre for High-End Computing (ICHEC), Tower Building, Trinity Technology & Enterprise Campus, Grand Canal Quay, Dublin 2, Ireland

L. A. A. Nikolopoulos

School of Physical Sciences, Dublin City University, Collins Ave, D9, Dublin, Ireland

National Centre for Plasma Science and Technology, NCPST, Collins Ave, D9, Dublin, Ireland

## Abstract

In this article we discuss two mutually beneficial ways of improving the computational tractability of TDSE calculations. In the first, the RMT approach for  $H_2^+$  which was developed is discussed. It is the first derivation and implementation of a Time-Dependent R-Matrix approach on a molecular system. This method involves the division of the molecular system into two regions which use different representations; an energy eigenstate representation in an inner region and a grid representation in an outer region [1]. The second area is on the use of GPGPU techniques applied to basis and grid approaches as well the molecular RMT approach. Specifically, the Arnoldi-Lanczos (Krylov Subspace), Runge-Kutta, Taylor series approaches to propagating the interaction of the light pulses with the atomic/molecular system as well as a GPU parallelisation related to the RMT method [2, 3].

## Introduction

Within computational atomic physics, significant progress has been occurring in terms of the sophistication of computational models and the compute power available in modern HPC systems. Recent advances in Time Dependent R-Matrix have also been made, such as work on double ejection. The computational challenges remain immense. While there have been technical advances in compute systems, the physics hasn't remained a stationary target. New advances such as HHG and FEL have led to new challenges such as modelling the behaviour of attosecond pulses and very-intense pulses on atomic and molecular systems. Even today, the *ab-initio* propagation of a hydrogen atom interacting with an intense ultra-short laser pulses generated by Titanium Sapphire lasers ( $\lambda \approx 800$  nm) a computationally massive problem. As one moves into the infrared regime ( $> 1200$  nm), the problem can become computationally intractable. This is due to an explosion of size in the state space required to approximate the system.

For molecular systems, the challenges are even greater than in atomic systems due to the loss of rotational symmetry. There are two key but orthogonal approaches to ameliorating these problems; more sophisticated computational models and advanced optimisation strategies using cutting-edge HPC hardware. Both approaches can unlock spectacular improvements in performance. As a result, our work has involved these two main strands in helping to investigate fundamental processes in laser-matter interactions. In the following two sections we briefly discuss work in both areas.

## RMT Theory for Molecules

In *ab-initio* simulations of single-electron atoms and molecules in intense laser fields, the TDSE is solved with as few approximations as possible. There are two popular approaches for solving the systems (amongst others).

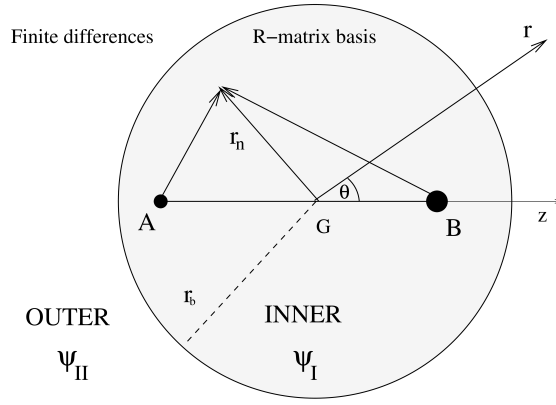


Figure 1: The division of space with an inner region with an B-spline energy eigenstate representation and an outer region with a grid representation using finite-differences. The dotted line is of length  $r_b$  and represents the radius from the centre which is marked  $G$  to boundary.  $r_n$  is the radius of the  $n$ th electron from the centre. The nuclei are marked  $A$  and  $B$ . The distance from  $A$  to the  $n$ th electron is  $|r_n - r_a|$  while the distance is  $|r_n - r_b|$  for the other nuclei. (from [1])

One approach is to consider the system in terms of energy eigenstates. If the system is initially in its ground state then the laser field couples other states. The electron wavefunction is then described by some linear combination of eigenfunctions:  $\sum_{\gamma} C_{\gamma}(t)\Phi_{\gamma}(\mathbf{r})$  where each eigenfunction has an associated energy  $E_{\gamma}$ . These field-free eigenfunctions are pre-calculated and the unknown quantities are the associated time-dependent coefficients.

The other approach is a grid approach. The wavefunction is now represented in terms of angular momenta components:  $\sum_{\gamma} \frac{1}{r} f_l(\mathbf{r}, t) Y_{lm}(\Omega)$ . In the energy eigenbasis approach the time dependence is contained in a function which only depends on time:  $C_{\gamma}(t)$  but the grid approach is dependent on  $f_l(\mathbf{r}, t)$ .

In the first case the laser field coupling is represented by an ODE with matrix structure which is block tridiagonal where the off-diagonal blocks are full. In the grid representation case, one has a sparse matrix. Both equations can be solved by generic methods to solve differential equations. The Taylor series method, the family of Runge-Kutta methods and the Arnoldi-Lanczos (Krylov subspace) approach are often used.

In the calculation of atomic and molecular systems, the wavefunction is set to only be present within a specific region. This is equivalent to modifying the central potential with a radial boundary which is infinitely high so that the system is in an infinite spherical well, i.e putting the system in a box. The radius of the box should be large enough so the system is not significantly modified by the box, whether that be from significantly distorted eigenstates or unphysical reflections of wave-packets back into the system. Seeing if the box size and discretisation is suitable can be tested by increasing the size of the box and decreasing the spacing during repetitions of the same calculation. The box can be taken as having no discernible effect if the results are converged. The effect of the box is to select only those continuum states which are zero on the boundary, so that the state of the system is now a summation over bound and discretised ionisation states and the discretised-continuum states are now square-integrable since they are necessarily zero outside of the box. This means the states can also be normalised, so that the normalisation criteria holds. The grid spacing also limits the highest energies which can be represented (by Nyquist's theorem).

Considering the bound energies are also limited in value depending on the specific B-spline and grid, the summations can be notationally unified into a single sum over the energy index,  $n$ :

$$\Psi(r, t) = \sum_n C_{n\lambda}(t) \sum_{l \in l_{\lambda}} Y_{l0}(\Omega) \frac{1}{r} P_{nl}(r), \quad (1)$$

where  $\lambda$  indicates the symmetry, gerade (g) or ungerade (u), and  $\sum_{l \in \lambda}$  indicates a sum over all angular momentum components of the symmetry, specifically a sum over even ( $\lambda = g$ ) or odd ( $\lambda = u$ ) numbers. In the RMT approach the basis and grid approaches are propagated simultaneously in different regions of the “box”. This is done by dividing the molecular system into two regions as shown in figure 1, an inner-region which uses a basis expansion and an outer-region which uses finite differences on a grid. The arbitrary value the wavefunction can take at the inner-region boundary between the regions means that the Hermiticity of the basis is lost. The RMT approach uses a neat Bloch-operator trick at the boundary to make the system’s Hamiltonian Hermitian and so the eigenfunctions and eigenvalues one calculates are real <sup>1</sup>. It’s important to note that unlike the atomic case, the angular momentum does not with the Hamiltonian operator, so the coupling of partial waves doesn’t have the same one-to-one correspondence as it does in one-electron atoms. Rather, each energy eigenstate is decomposed into partial wave components <sup>2</sup>. This allows for the modelling of the probability density flux flowing through from the inner region to the outer. The RMT approach was tested by comparing calculations to literature values, checking the simulation was agnostic to the boundary position and checking that basic laser-physics features were replicated. This treatment is done with the future aim of separating multi-electron dynamics in the inner region from one-electron dynamics in the outer region; this will massively reduce the dimensionality problems of multi-electron molecular systems.

The eigenvalues and eigenvectors from the Bloch-augmented TDSE don’t correspond to the physical system, so the actual ground state of the system is described as a mixture of these Bloch-augmented states. The ground state is calculated by propagating the Bloch-augmented states with complex time propagation of the (augmentation corrected) TDSE. This causes the underlying lowest lying energy state to grow at a rate of  $e^{|E\gamma|}$ . With some propagation and normalisation steps, the system settles into the ground state. During this process, one can see probability flux flowing through the boundary and across the partial waves.

The case for using the RMT approach for  $H_2^+$  is stronger than in the hydrogen case due to an increase of the dimensionality problems in the basis method. The number of eigenstates scales with the square of the radius and the square of the number of angular momenta terms (i.e  $N^2 L^2$  compared to  $N^2$ ) due to the loss of rotational symmetry in the central potential. Calculations up to 3000 atomic units are feasible for Hydrogen, for  $H_2^+$  diagonalisation and propagation of the basis with any significant number of L, it is not currently possible. This problem does not exist in the RMT case. We limit the size of the basis to the inner region. This provides us with the flexibility of knot points etc and precision from B-spline basis methods. The finite difference outer region lends itself to a very powerful approximation at large distance; a key advantage of a grid representation is that a molecular potential can be approximated by a hydrogenic target at a sufficient distance from the nuclei. A hydrogenic potential does not couple terms in the central potential and thus reduces memory and computational requirements significantly. This makes the large distances comparative to the hydrogen basis realisable.

## CLTDSE

The code written from scratch for the current work is known as CLTDSE. It’s primary function is to implement methods for the time propagation of atomic and molecular quantum systems under the interaction of laser fields which are described classically (i.e the semi-classical approximation). For this, three representations of the quantum system are directly supported:

- Basis Methods
- Finite Difference
- RMT (mixed-methods)

---

<sup>1</sup>Our matrix is actually now symmetric

<sup>2</sup>see [1] for the specific equations which govern the system

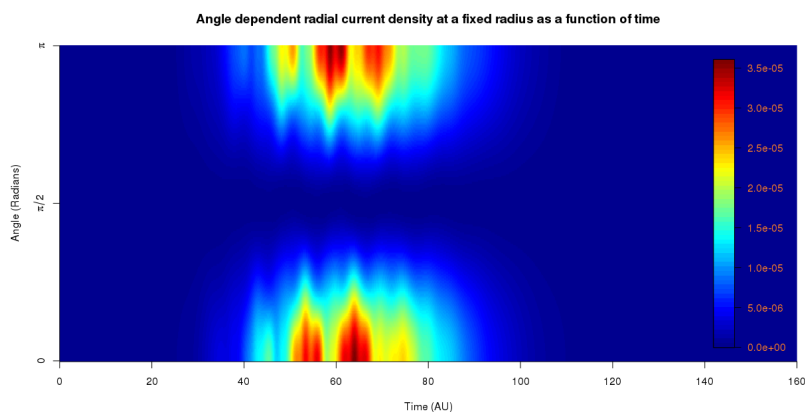


Figure 2: An example output from CLTDSE. The strength of the time-dependent radial probability current  $j_r(r_b, \Omega, t)$  at a fixed radius  $r_b = 9.98$  a.u. and for  $\theta$  from 0 to  $\pi$ , over the duration of the pulse. The pulse was a  $1 \times 10^{15}$  W/cm<sup>2</sup>, 10 eV and 10 cycle sine-squared pulse. Since  $m = 0$ , the angle,  $\phi$ , plays no role. (from [3])

For the RMT and basis methods, the code also includes an ability to solve the time-independent Hamiltonian for H and H<sub>2</sub><sup>+</sup> using a B-spline basis. Relevant data, such as B-spline coefficients, eigenenergies radial eigenfunctions or components of the radial eigenfunction expansion (H<sub>2</sub><sup>+</sup>), are written to a NetCDF format. For the RMT and finite difference, support is also required for solving the diffusion equation for the ground state eigenenergy.

For solving the TISE and TDSE, 3 methods are supported:

- The Taylor-expansion method
- The family of Runge-Kutta methods <sup>3</sup>.
- The Arnoldi-Lanczos approach to shrinking the Hamiltonian matrix to a subspace where only a few basis vectors are required.

The basis and finite difference methods support all three approaches, while the RMT work focusses on the Taylor expansion. For the TDSE solution, a variety of laser pulses are also implemented in the code, from Trapezoidal, Sine-squared and Gaussian pulses, to pulses imported directly from real lasers pulses (using interpolation to support different time-steps), to pulses generated from a variety of stochastic approaches. The velocity-gauge vector potential is also supported through direct numerical integration.

A number of post-propagation analysis functionality is also supplied for all three representations. This includes the standard yield, ground state population etc, but also more interesting calculations such as the angle-dependent yield and the probability density as shown in Fig. 2 for Hydrogen. The figure shows how the orientation of the field along the z-axis induces probability flux to flow outwards parallel with the orientation of the laser field (which alternatives between being parallel and anti-parallel with the z-axis) at that time. The effect of the laser pulse stripping away probability density away from the atomic or molecular system is shown particularly clearly in this view.

## GPGPU

All major clusters or supercomputers consist of many nodes. Each node itself consists of one or more processors which have multiple cores. These nodes now often have accelerators such as graphic cards. The

<sup>3</sup>RK4, RKF-4(5), Merson, Cash-Karp, Radau, Dormand-Prince etc

nodes, which are increasingly heterogeneous, are interconnected through a high speed network that has a specific topology. These topologies vary depending on the specific system.

In the past two decades there have been several advances in various directions in the state of the computational infrastructure available. This includes reliable and robust numerical libraries, sophisticated compilers, high speed inter-connected nodes with high bandwidth memory and HPC capabilities as well as visualisation software. The emergence of CPU-based parallel architectures allowed the development of High Performance Fortran, various parallel versions of C++ and the successful usage of MPI and OpenMP. After the emergence of these commodity systems, HPC infrastructure has moved away from custom fully integrated systems towards distributed computing models. These rely heavily on interconnected commodity machines. Now, these distributed systems are being augmented with various forms of accelerators. Accelerators focus on optimising a specific class of problem and there is a growing interest in heterogeneous computational environments. In ICHEC and CINECA<sup>4</sup> this involves the use of pGPU to augment an efficient and low-cost, *distributed* hybrid computing system [4] as well as the use of other co-processors such as the Intel Phi as in ICHEC. The use of pGPU as computational accelerators is known as GPGPU. The focus for pGPU is on problems which are computationally heavy and throughput-focused rather than latency bound.

Currently GPGPU is focused on the use of discrete cards but with the current ongoing convergence between CPU and GPU it is expected that the trend is for GPGPU with double precision to be available on integrated chips and provide improved communication performance. The main benefit of the integration will be the lower latency and higher bandwidth between the GPU and CPU.

The GPGPU acceleration of simulations is a hot topic because of the flops per euro cost of GPUs in comparison to CPUs when looking at well-suited algorithms. Although originally for games, GPUs are many-core devices with a SIMD design. On a HPC system, the GPUs are a comparable price to their CPU counterparts on each node, while the performance achievable for scientific simulations may be orders of magnitude greater.

OpenCL is a modern compute-accelerator orientated language which has much similarity with CUDA except that it is not tied to a single vendor, but rather operates on hardware from NVIDIA, AMD, Intel, Xilinx, Altara etc and on devices from CPU, GPUs, Intel Phi and FPGA etc. Code is portable, but not performance portable, so significant architectural details are required when implementing code. Since 2010, accelerator availability on the top 500 HPC systems has risen from 9 in June 2010 to 85 by June 2015 with most being split between NVIDIA GPUs and the Intel Phi<sup>5</sup>.

Due to the explosion of GPGPU work from about 2007, double precision support has been available on the cards for some time, where full or near full IEEE-754 conformance appeared during the course of the work. Double precision is required for the calculation of atomic structure and in the subsequent time propagation under a light field<sup>6</sup>.

The opportunities are immense for our field because *ab-initio* methods for calculating the dynamics of light-matter interactions are generally very parallelisable as the core bottleneck is a matrix-vector problem with either full-blocks or known structure. The practical exploitation of GPU significantly reduced the runtime of the code. The basis approach is not particularly computationally dense, but the parallelisability of the algorithms and the fact that the data access pattern is highly uniform leads to a priority of high bandwidth over latency which perfectly suits the high bandwidth available while the very poor latency to the global memory of the GPU is masked.

GPU parallelisation efforts do not contribute by accelerating the integration method itself; the Runge-Kutta, Arnoldi-Lanczos and Taylor methods are serial, and the calculation of each derivative is done sequentially. That is, the methods require multiple derivatives to be calculated, where each new derivative calculation

---

<sup>4</sup>ICHEC is the national high performance computing centre for Ireland while CINECA is a facility in Bologna funded by a consortium of Italian universities.

<sup>5</sup><http://top500.org/statistics/overtime/>

<sup>6</sup>Unfortunately, GPU manufacturers (initially NVIDIA but also now AMD) limit double precision FLOPs on their consumer-grade cards.



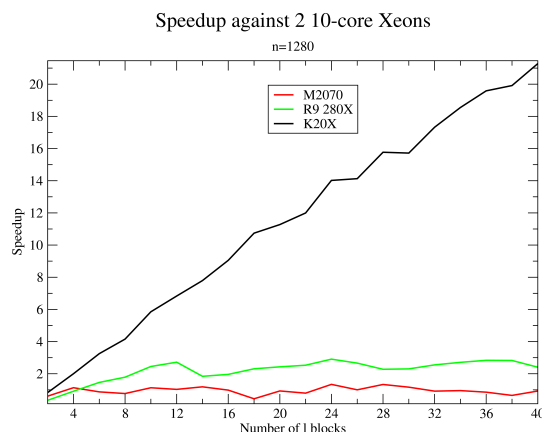


Figure 3: The speedup of the NVIDIA K20X, AMD R9 280X and NVIDIA M2070 in comparison to a  $2 \times 10$  core Intel Xeon's.

requires information from the previous derivative. Rather than using a parallel integration algorithm, the matrix vector calculation that is performed at each time step is, itself, parallelised. GPU are the natural partner to this form of embarrassingly-parallel, linear-algebra acceleration. All of the major portions of the time propagation approaches were performed directly on the GPU.

The grid approach can be done such that it is relatively computationally dense. After parallelising the code on a K20X GPU and exploiting intercache data locality by exploiting the Hermiticity of the problem, the performance improved about 20 times, as shown in 3 in comparison to a  $2 \times 10$  core Intel Xeons as the loads tested increased in size<sup>7</sup>. What is also interesting is that the AMD R9 280X, a commodity graphics card, was an order of magnitude cheaper than the Intel Xeons and the NVIDIA K20X. Although the performance didn't equal the K20X, it still reduced the runtime by half in comparison to 2 very expensive CPUs.

## Concluding statement

This work constitutes a significant advance in computational physics on two fronts.

From the creation of the RMT method in 2008 [5], work since has focused on various aspects of atomic systems [6, 7, 8] including recent double-ionization work [9]. In this article, we have discussed the first extension of RMT theory to molecules. The work has focused on  $H_2^+$  since it is the simplest molecular system. This extension reduces the dimensionality problems in  $H_2^+$ , since one can now have a full basis inner region and have a finite difference outer region which decouples the angular momenta terms as the hydrogenic approximation becomes valid ( $V(r) \approx V_H(r)$ ).

In the remainder of the article, the first native GPGPU-based *ab-initio* TDSE propagator for atoms and molecules in intense laser fields has been discussed. The propagator used the OpenCL framework to achieve large speedups on the GPU against OpenCL on the CPU. This makes problems more computationally realisable.

The introduction of multielectron dynamics in this work will be an exciting future development of the RMT approach, and the future usage of GPUs within the field will also significantly advance the feasible simulations available to researchers. MPI parallelism can be combined with GPU parallelism to provide mutually beneficial effects for scalability. MPI parallelism allows more nodes to be included at scale while a GPU can help reduce the load on a particular node. This heterogenous parallelism represents a new and exciting area for future study on *ab-initio* time propagation. Future work on both strands will have highly novel possibilities.

<sup>7</sup>The scaling had also not plateaued either, but rather our compute hours allocation had

## Acknowledgments

Thanks to funding from the European Seventh Framework under the code FP7-HPCAMO, thanks also to funding from COST CM1204 and MP1203. The authors would like to acknowledge P. Decleva & K. T. Taylor. C OB would like to acknowledge D. Dundas for assistance with comparison calculations and acknowledges the Irish Centre for High-End Computing (ICHEC) for the use of computational resources under Project No. dcphy005c. Partial financial support from COST CM1204 and MP1203 is also gratefully acknowledged.

## References

- [1] Cathal   Broin and L. A. A. Nikolopoulos. R-Matrix Incorporating Time method for  $H_2^+$  in Short and Intense Laser Fields. *Physical Review A*, 92:063428, 2015.
- [2] Cathal   Broin and L. A. A. Nikolopoulos. An OpenCL implementation for the solution of the time-dependent Schr odinger equation on GPUs and CPUs. *Computer Physics Communications*, 183(10):2071–2080, 2012.
- [3] Cathal   Broin and L. A. A. Nikolopoulos. A GPGPU based program to solve the TDSE in intense laser fields through the finite difference approach. *Computer Physics Communications*, 185(6):1791–1807, 2014.
- [4] S J Pennycook, S D Hammond, G R Mudalige, S A Wright, and S A Jarvis. On the Acceleration of Wavefront Applications using Distributed Many-Core Architectures. *Comput. J.*, 55(2):138–153, July 2011.
- [5] L. A A Nikolopoulos, J. S Parker, and K. T Taylor. Combined R-matrix eigenstate basis set and finite-difference propagation method for the time-dependent Schr odinger equation: The one-electron case. *Phys. Rev. A*, 78(6):063420, December 2008.
- [6] L.R. Moore and M.A. Lysaght and L.A.A. Nikolopoulos and J.S. Parker and H.W. van der Hart and K.T. Taylor. The RMT method for many-electron atomic systems in intense short-pulse laser light. *J. Mod. Opt.*, 58(13):1132–1140, 2011.
- [7] L. R. Moore, M. a. Lysaght, J. S. Parker, H. W. van der Hart, and K. T. Taylor. Time delay between photoemission from the 2p and 2s subshells of neon. *Phys. Rev. A*, 84(6):61404, December 2011.
- [8] M A Lysaght, L R Moore, L A A Nikolopoulos, J S Parker, H W Hart, and K T Taylor. Ab Initio Methods for Few- and Many-Electron Atomic Systems in Intense Short-Pulse Laser Light. In Andr e D. Bandrauk and Misha Ivanov, editor, *Quantum Dyn. Imaging*, CRM Series in Mathematical Physics, pages 107–134. Springer New York, 2011.
- [9] Jack Wragg, JS Parker, and HW van der Hart. Double ionization in r-matrix theory using a two-electron outer region. *Physical Review A*, 92(2):022504, 2015.

# Tensor Networks and Geometry for the Modelling of Disordered Quantum Many-Body Systems

Andrew M. Goldsborough

✉ andrew.goldsborough@mpq.mpg.de

Max Planck Institute for Quantum Optics, Hans-Kopfermannstr. 1, D-85748 Garching, Germany

Department of Physics and Centre for Scientific Computing, The University of Warwick, Coventry, CV4 7AL, United Kingdom

Rudolf A. Römer

✉ r.roemer@warwick.ac.uk

Department of Physics and Centre for Scientific Computing, The University of Warwick, Coventry, CV4 7AL, United Kingdom

## Introduction

At its most fundamental level a quantum many-body system can be defined by a Hilbert space  $\mathcal{H}$  and a Hamiltonian  $H$  describing the evolution of states in  $\mathcal{H}$ . But with  $\sim 2^{10^{23}}$  states for just a single mole of, e.g., spin-1/2 particles, computing ground states and excitations remains a formidable challenge. Fortunately, advanced numerical methods have been developed in the last decades to tackle the problem. Whilst density-functional theory, dynamical mean-field theory, quantum Monte Carlo and their variants and extensions have allowed us to study systems with hundreds – and sometimes thousands – of atoms in three dimensions, large strongly correlated systems are more problematic. However, much has been learned in low dimensional systems by applying concepts from quantum information to many body physics. At the heart of this understanding lies the realization that not all states in  $\mathcal{H}$  are equal in terms of their entanglement properties. For a general state in  $\mathcal{H}$  the entanglement entropy  $S_{A|B}$  scales as the *volume* of subsystem. However, for ground states of *gapped* systems, the entanglement scales as the *area* of the boundary separating the subsystems. This is the famous *area law* for entanglement entropy [1, 2, 3]. It suggests that much of the low energy physics is likely to be well described by a much smaller, area law satisfying subset of  $\mathcal{H}$ . The success of tensor network methods is down to their ability to capture the entanglement described by the area law and provide a variational ansatz within the space of area law satisfying states [4]. The simplest tensor network, the matrix product state (MPS), is at the heart of the density matrix renormalisation group (DMRG) algorithm, accepted to be the most accurate approach for the numerical study of strongly correlated 1D systems [5]. In 2D, one has to use more sophisticated tensor networks such as projected entangled pair states (PEPS) to make progress.

The area law for  $S_{A|B}$  in quantum-many body systems was foreshadowed in the theory of black hole thermodynamics. It had been found [6, 7] that black holes have a thermal Bekenstein-Hawking entropy  $S_{BH} = \frac{\mathcal{A}_h}{4G}$ , that scales with the surface area  $\mathcal{A}_h$  of the black hole horizon;  $G$  is Newton's gravitational constant. For  $S_{A|B}$ , Ryu and Takayanagi [8] suggest a similar extension in the context of the so-called AdS/CFT correspondence, i.e. the duality between quantum gravity on a  $D + 2$  dimensional Anti-de Sitter (AdS) spacetime and a conformal field theory (CFT) defined on its  $D + 1$  dimensional boundary [9]. The entanglement entropy of a region  $A$  of the CFT is related to the size of the surface with smallest area, or *minimal surface*  $\gamma_A$ , within the AdS bulk that separates  $A$  from the rest of the system. This is shown pictorially in fig. 1. In condensed matter systems, AdS/CFT can provide a geometric interpretation of the renormalization group (RG) approach. The additional *holographic* dimension can be interpreted as a scale factor in the RG coarse graining [10]. This analogy gives  $S_{A|B} = \frac{\mathcal{A}_{\gamma_A}}{4G_N^{(D+2)}}$ , where  $\mathcal{A}_{\gamma_A}$  is the area of the minimal surface  $\gamma_A$  and  $G_N^{(D+2)}$  is Newton's constant in  $D + 2$  dimensions. As we shall see, these concepts underpin the success of tensor networks that satisfy the area law and beyond.

For disordered *and* interacting systems, the variational refinement of tensor networks can already be too costly and has to be balanced with the need to additionally average of many, sometimes thousands of

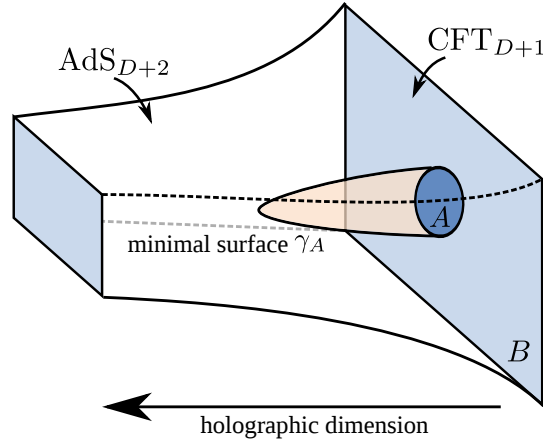


Figure 1: A diagrammatic representation of the AdS/CFT correspondence, showing a  $(D + 1)$  dimensional CFT on the boundary of a  $(D + 2)$  dimensional AdS spacetime. The entanglement entropy of a region  $A$  of the CFT is proportional to the minimal surface  $\gamma_A$  that separates  $A$  from the remainder of the CFT.

disorder realizations. As we will show here, instead of variationally refining a particular tensor network, a strategy that self-assembles the tensors according to a physically motivated, realisation-specific disordered network provides a viable alternative strategy.

## Matrix Product States

Consider a quantum system with basis states  $|\uparrow\rangle$  and  $|\downarrow\rangle$  for each site in a system with  $L$  sites. Simple *product states* can be formed as tensor product of the bases [11], for example  $|\uparrow\rangle \otimes \cdots \otimes |\uparrow\rangle$ . For, e.g.  $L = 2$ , any state can be written as a superposition of all possible two site product states,

$$|\Psi\rangle = (u_1 |\uparrow\rangle + d_1 |\downarrow\rangle) \otimes (u_2 |\uparrow\rangle + d_2 |\downarrow\rangle) = \sum_{\sigma_1, \sigma_2} C_{\sigma_1, \sigma_2} |\sigma_1\rangle \otimes |\sigma_2\rangle, \quad (2)$$

where  $\sigma_i$  can be  $\uparrow$  or  $\downarrow$ ,  $u_i, d_i$  are numerical coefficients and  $C_{\sigma_1, \sigma_2}$  is a two component tensor with elements

$$\mathbf{C} = \begin{pmatrix} u_1 u_2 & u_1 d_2 \\ d_1 u_2 & d_1 d_2 \end{pmatrix}. \quad (3)$$

Product states such as (2) have bases independent of each other and the expectation values factorise. On the other hand, *entangled* states such as

$$|\Psi\rangle = \frac{1}{\sqrt{2}} (|\uparrow\rangle \otimes |\downarrow\rangle - |\downarrow\rangle \otimes |\uparrow\rangle) \quad (4)$$

do not have factorising expectation values. The maximally entangled state (4) would require a tensor of the form

$$\mathbf{C} \equiv \begin{array}{c|cc} & \sigma_2 = \uparrow & \sigma_2 = \downarrow \\ \hline \sigma_1 = \uparrow & 0 & 1/\sqrt{2} \\ \sigma_1 = \downarrow & -1/\sqrt{2} & 0 \end{array} = \frac{1}{\sqrt{2}} \begin{pmatrix} 0 & 1 \\ -1 & 0 \end{pmatrix}, \quad (5)$$

which cannot be described by the coefficients  $u_1, d_1, u_2$  and  $d_2$  in eq. (3). Instead, let us introduce matrices [12],

$$\mathbf{M}_1 = \frac{1}{\sqrt{4}} \begin{pmatrix} 1 & 0 \\ 0 & 1 \end{pmatrix}, \quad \mathbf{M}_2 = \frac{1}{\sqrt{4}} \begin{pmatrix} 0 & 1 \\ -1 & 0 \end{pmatrix}. \quad (6)$$

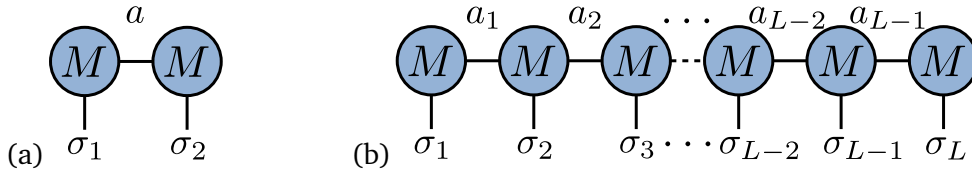


Figure 2: Diagrammatic representation of (a) the two site MPS in eq. (7) and (b) the general  $L$  site MPS of eq. (8). The circles represent the  $M$  tensors and the lines are the tensor indices. The horizontal lines represent the bond indices, the vertical lines the physical indices.

These matrices, combined using a standard matrix product, can easily produce the entangled state

$$C_{\sigma_1, \sigma_2} = \sum_a [\mathbf{M}_1]_a^{\sigma_1} [\mathbf{M}_2]_a^{\sigma_2} \Rightarrow \mathbf{C} = \frac{1}{\sqrt{2}} \begin{pmatrix} 0 & 1 \\ -1 & 0 \end{pmatrix}, \quad (7)$$

as desired. The  $a$  index introduces entanglement between the two states and can be thought of as a form of *bond*. Note that we have chosen the upper and lower placement of the indices for later convenience. Eq. (7) defines the simplest *matrix product state* (MPS). It can be expressed diagrammatically as in fig. 2(a), where the matrix is drawn as a circle and each index is represented by a line or *leg*. The matrix multiplication, or more generally tensor contraction, is shown by joining the lines that represent the summed over index. These diagrammatic representations of the state become very convenient for larger and more complicated tensor networks and are commonplace in the literature.

A general wavefunction on a lattice of  $L$  sites can be written as  $|\Psi\rangle = \sum_{\sigma_1, \dots, \sigma_L} C_{\sigma_1 \dots \sigma_L} |\sigma_1\rangle \otimes \dots \otimes |\sigma_L\rangle$ . As with the two site case, the  $C_{\sigma_1 \dots \sigma_L}$  tensor can be split into a series of local tensors with connections to their neighbours that allow the inclusion of entanglement. When away from boundaries each site has two neighbours thus the tensors at each site have three indices; one for the site basis and one for each neighbour. In full the wavefunction takes the form

$$|\Psi\rangle = \sum_{\sigma_1, \dots, \sigma_L} \sum_{a_1, \dots, a_{L-1}} M_{a_1}^{\sigma_1} M_{a_1 a_2}^{\sigma_2} \dots M_{a_{L-2} a_{L-1}}^{\sigma_{L-1}} M_{a_{L-1}}^{\sigma_L} |\sigma_1, \dots, \sigma_L\rangle, \quad (8)$$

where  $|\sigma_1 \dots \sigma_L\rangle \equiv |\sigma_1\rangle \otimes \dots \otimes |\sigma_L\rangle$  and  $M_{a_{i-1} a_i}^{\sigma_i} \equiv [\mathbf{M}_i]_{a_{i-1} a_i}^{\sigma_i}$ . The  $\sigma_i$  indices label the spins of the basis and are known as the *physical indices*, whereas the  $a_i$  are the *bond, virtual or auxiliary indices*. To draw a distinction between the two index types, it is convention to have the physical  $\sigma_i$  as upper indices, thus giving the standard form of an MPS [5]. As before, the MPS can be represented diagrammatically as a chain of circles connected horizontally by the bond indices and with the physical indices drawn vertically as in fig. 2(b). Note that (8) corresponds to a state with open boundary conditions (OBCs) as is evident from the special tensors  $M_{a_1}^{\sigma_1}$  and  $M_{a_{L-1}}^{\sigma_L}$  at the sites 1 and  $L$ .

The MPS (8) is an exact representation of any state in  $\mathcal{H}$ . When increasing site index  $i$  up to the centre of the chain, the size of each  $M_{a_{i-1} a_i}^{\sigma_i}$  increases. For example when  $i = L/2$  the dimensions of the MPS tensor are  $[d, d^{\frac{L}{2}-1}, d^{\frac{L}{2}}]$ , where  $d$  is the dimension of the site basis, e.g.  $d = 2$  for spin-1/2 systems. This means that the number of elements of the centre tensor is  $d^L$  as expected when all of the information is preserved. By limiting the size of the bond indices, known as setting the *bond dimension*  $\chi$ , one truncates the size of the Hilbert space allowing much larger system sizes to be computationally tractable. Setting  $\chi$  also controls the amount of entanglement that the wavefunction (8) can have. Due to the fact that ground states of gapped Hamiltonians satisfy the area law, and therefore have relatively little entanglement, setting a finite  $\chi$  still allows for an accurate description of the wavefunction. For example, while exact diagonalisation is usually limited to  $L \sim 30$  sites [13], the MPS approach can study many hundreds of sites with  $\chi \sim \mathcal{O}(10^3)$  [14]. The MPS can be used as a variational ansatz by *sweeping* back and forth across the chain choosing the contents of each  $M_{a_{i-1} a_i}^{\sigma_i}$  that minimises the energy. This variational MPS algorithm is often referred to as DMRG, despite the fact that the original DMRG algorithm [15] does not use an MPS. A full discussion of MPS based DMRG can be found in reference [5].

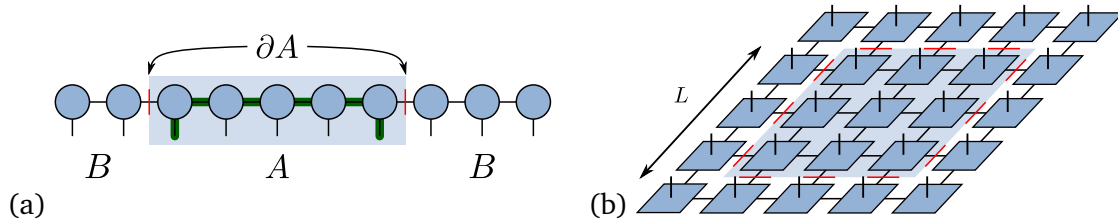


Figure 3: (a) For an MPS a region  $A$  (shaded blue) is bounded by two bonds, denoted by red lines. If the size of  $A$  is increased the number of bonds stays at 2. The bold green line highlights the minimum path between two sites. (b) A PEPS on a square lattice, where the PEPS tensors are blue squares, the virtual indices are in the plane, and the physical indices are those pointing up. As before, the region under consideration is highlighted in blue and the bonds that separate it from the rest of the system are shown by red lines. Here the boundary scales as  $4L$  and is therefore area law conserving.

## Tensor networks

### The Area Law for Entanglement Entropy

As highlighted in the introduction, the area law states that the entanglement entropy for ground states in gapped quantum many body systems scales with the boundary of a subsystem rather than the volume. This means that these ground states are significantly easier to simulate on a classical computer than generic states. For tensor networks the *boundary* is quantified by the number of bonds  $n_A$  connecting region  $A$  to the environment  $B$ . The reasoning behind this measure is that if all of the tensors are identical, with a bond dimension  $\chi$  the maximum contribution to the entanglement entropy per bond is  $\log_2(\chi)$ . Evenbly and Vidal [16] go further to suggest that for most cases of homogeneous tensor networks the entanglement per bond is approximately 1, hence  $S_{A|B} \approx n_A$ . The boundary of a region in a 1D system is simply two points and does not increase when the region is expanded. An MPS has these same properties; the number of bonds that one would have to cut to separate region  $A$  from  $B$  is 2 and does not change if the size of  $A$  is altered, as shown in fig. 3(a). The fact that the MPS has the same entanglement properties as the ground state of a gapped 1D system makes it an ideal variational ansatz for such problems and gives a reason for the excellent scaling for these systems.

The area law also explains why performance of DMRG for critical and 2D systems is worse. For critical systems the entanglement entropy scales logarithmically with the region size,  $S_{A|B} \propto \log(L)$  [17, 18], hence the  $\chi$  required for accurate DMRG increases with system size. For 2D, take for example a square lattice with a square region within it. If the region has side length  $L$ , the area law suggests that the entanglement entropy should scale as its boundary  $S_{A|B} = 4L \propto L$ , thus the MPS is insufficient as a variational ansatz for this system. An area law conserving ansatz would be a tensor network where all sites are connected to their four neighbours to match the lattice geometry, as shown in fig. 3(b). This tensor network is known as a *projected entangled pair state* (PEPS) and is can be viewed as natural 2D extension of the MPS [19, 20].

### Beyond the Area Law

Tensor networks, particularly the multi-scale entanglement renormalisation ansatz (MERA) [21, 22], can be seen as a coarse grained embodiment of AdS/CFT [16, 23]. The structure of MERA, shown in fig. 4(a), is made up of *disentanglers* (green squares) and *isometries* (pink triangles). The intuitive argument behind its construction is that the disentanglers remove short range entanglement so that the isometries can then remove degrees of freedom that are no longer coupled to the system. The network is self-similar in the way that at each level of coarse graining the network looks the same. This direction of coarse graining, perpendicular to the physical lattice, is the extra *holographic* dimension.

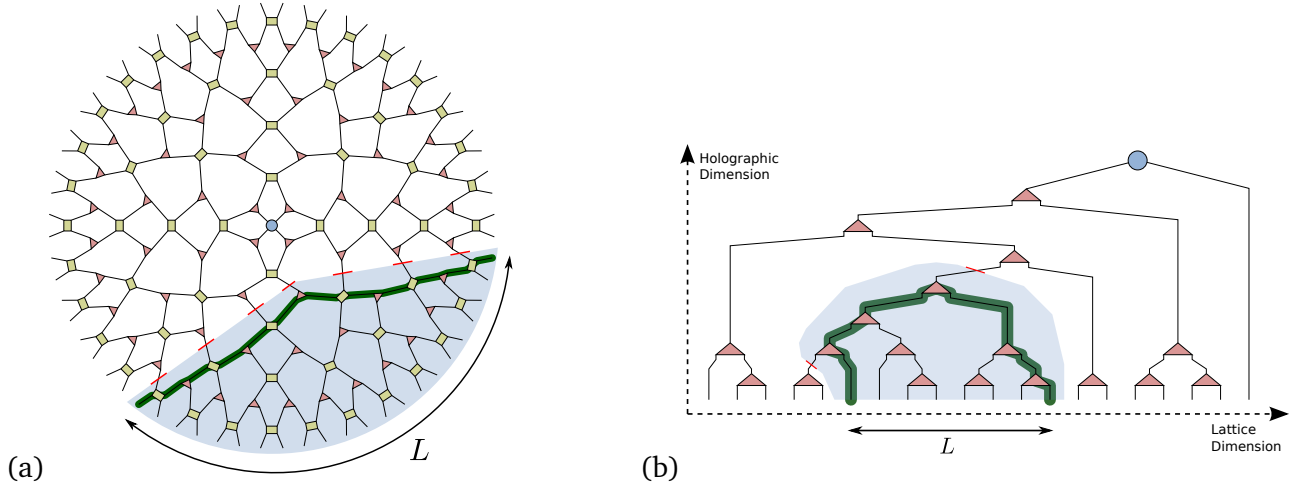


Figure 4: (a) Tensor network diagram of a MERA with periodic boundary conditions where the green squares are *disentangler*s, pink triangles are *isometries* and the blue circle is the top tensor. A region of the network corresponding to  $L$  sites is highlighted in blue, where the bonds making up the minimum surface are highlighted by the red lines. The bold green line highlights a *geodesic* connecting two points on the lattice. (b) The SDRG algorithm as a TTN for a chain of  $L = 20$  sites. Shapes and lines are as in (a). Lattice and holographic dimensions are indicated by the dashed arrows.

Just as with MPS and PEPS, the minimal surface  $\gamma_A$  is found by counting the minimum number of bonds that have to be cut to separate one region from the rest of the system. Take, for example, a region comprised of  $L$  sites within a MERA as shown in fig. 4(a). The minimum number of bonds (red lines in fig. 4(a))  $n_A \approx \log(L)$ , which matches the entanglement scaling of critical systems [16]. As an extension of this, it was shown [24, 25] that in the continuum limit of MERA it has a metric that matches the properties of AdS/CFT.

In addition to entanglement entropy, similar arguments hold for two-point correlation functions [23, 16]. The asymptotic scaling of correlation functions should be

$$C_{\text{TN}}(x_1, x_2) \sim e^{-\alpha D_{\text{TN}}(x_1, x_2)}, \quad (9)$$

where  $D_{\text{TN}}$  is the path with the minimum distance or *geodesic* connecting points  $x_1$  and  $x_2$  within the tensor network. For MPS  $D_{\text{MPS}} = |x_2 - x_1|$ , as shown as the bold line in fig. 3(a). Hence

$$C_{\text{MPS}}(x_1, x_2) \sim e^{-\alpha D_{\text{MPS}}(x_1, x_2)} = e^{-|x_2 - x_1|/\xi}, \quad (10)$$

where  $\xi$  is the correlation length. MERA, on the other hand has path lengths that scale logarithmically with separation of  $x_1$  and  $x_2$  ( $D_{\text{MERA}}(x_1, x_2) \propto \log_2(L)$ ), as shown in fig. 4(a). Thus

$$C_{\text{MERA}}(x_1, x_2) \sim e^{-\alpha D_{\text{MERA}}(x_1, x_2)} = |x_2 - x_1|^{-q}, \quad (11)$$

recovering the power law decay profile characteristic of critical systems.

## Structurally inhomogeneous tensor networks

For *disordered* quantum many-body systems, the strong-disorder renormalisation group (SDRG) provides a powerful means of analysing a system by concentrating principally on the disorder within it. The approach was originally devised by Ma, Dasgupta and Hu [27, 28] for the random anti-ferromagnetic (AFM) Heisenberg chain where the coupling constant is different for each position, taking a random value. The



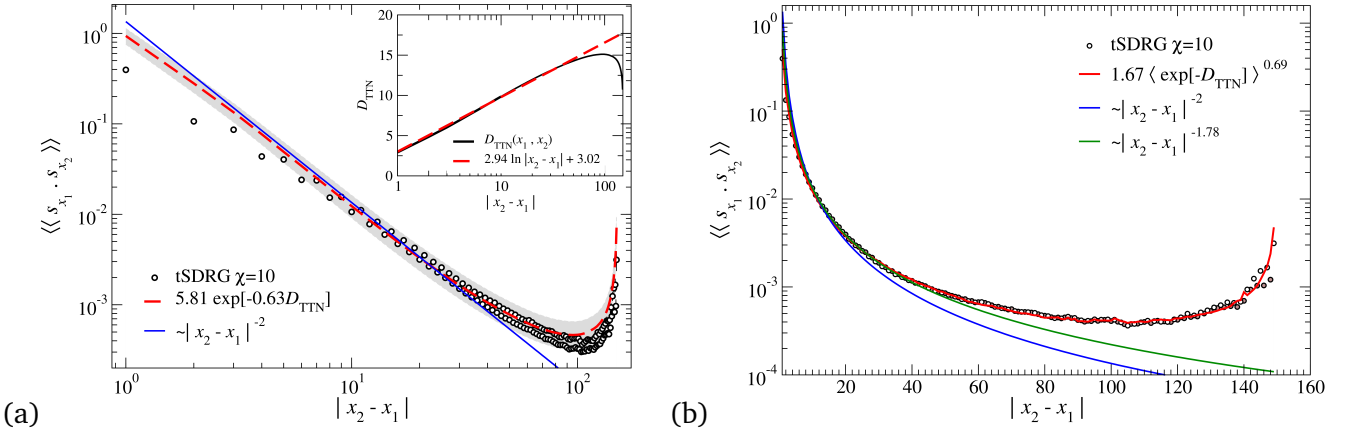


Figure 5: (a) Reproduced from [26]. Correlation function for  $L = 150$  averaged over 2000 samples for the direct calculation of  $\langle\langle \vec{s}_{x_1} \cdot \vec{s}_{x_2} \rangle\rangle$  (black circles) and also via the holographic approach (12) using  $D_{\text{TTN}}$  (dashed red line with error of mean indicated by the grey shading) such that  $\langle\langle \vec{s}_{x_1} \cdot \vec{s}_{x_2} \rangle\rangle \approx (5.81 \pm 0.93) \exp[-(0.62 \pm 0.02) D_{\text{TTN}}]$ . The expected thermodynamic scaling  $|x_2 - x_1|^{-2}$  is also shown (solid blue line). Inset: The holographic path length  $D_{\text{TTN}}$  connecting sites  $x_1$  and  $x_2$  averaged over the 2000 TTNs (black) and a fit in the logarithmic regime (red). (b) Rescaled correlation function to remove odd-even effects on a semi-log plot. The expected thermodynamic scaling is shown as a solid blue line. The fitted scaling factor from (a) is plotted as a solid green line. The red line indicates the alternative holographic fitting with  $\langle\langle \vec{s}_{x_1} \cdot \vec{s}_{x_2} \rangle\rangle \approx (1.67 \pm 0.10) \langle \exp[-D_{\text{TTN}}] \rangle^{(0.69 \pm 0.01)}$ .

principle behind the SDRG is to eliminate the most strongly coupled pairs of spins and replace them with an effective interaction that couples the spins at either side. The most strongly coupled pair are thought of as being *frozen* into a singlet ground state as the neighbouring interactions are significantly weaker – ultimately leading to the random singlet phase, which is the ground state of the system [29]. This freezing out of pairs of sites is conceptually similar to the removal of local degrees of freedom in MERA and also suggests the possible usefulness of concepts from AdS/CFT for disordered spin chains.

The SDRG method was extended by Hikihara et. al. [30] to include higher states at each decimation, in the spirit of Wilson’s numerical renormalisation group [31] and DMRG [15]. This method therefore decomposes the system into blocks rather than larger spins allowing for more accurate computation of, e.g., spin-spin correlation functions. The more states that are kept at each decimation the more accurate the description and it is exact in the limit of all states kept. This *numerical SDRG* amounts to a coarse-graining mechanism that acts on the operator. We show in reference [26] that it is equivalent to view this as a multi-level tensor network wavefunction acting on the original operator. The operators that coarse-grain two sites to one can be seen as *isometric tensors* or *isometries* that satisfy  $ww^\dagger = \mathbb{1} \neq w^\dagger w$ . When viewed in terms of isometries, the algorithm can self-assemble a tensor network based on the disorder of the system. When written in full, it builds an inhomogeneous binary tree tensor network (TTN) as shown in fig. 4(b). We shall henceforth refer to this TTN approach to SDRG as *tSDRG*. For a full description of the algorithm see reference [26].

## Correlation Functions

The correlation functions for a strongly disordered Heisenberg chain are expected to disorder-average to a power-law decay with power  $|x_2 - x_1|^{-2}$  [29]. As discussed in the previous section, correlation functions in tensor networks scale as  $e^{-\alpha D(x_1, x_2)}$ , where  $D(x_1, x_2)$  is the number of tensors that connect site  $x_1$  to  $x_2$  [16], for example  $D(6, 13) = 5$  in fig. 4(b) highlighted in green. tSDRG has a holographic geometry based on a random TTN, with average path length  $\langle D_{\text{TTN}} \rangle \approx \log |x_2 - x_1|$ , i.e. scaling logarithmically with



distance. This makes it ideally suited to capture the desired power law decay

$$\langle\langle \vec{s}_{x_1} \cdot \vec{s}_{x_2} \rangle\rangle \sim e^{-\alpha \langle D_{\text{TTN}}(x_1, x_2) \rangle} \sim e^{-\alpha \log|x_2 - x_1|} \sim |x_2 - x_1|^{-a}. \quad (12)$$

In fig. 5(a), we show the behaviour of  $\langle\langle \vec{s}_{x_1} \cdot \vec{s}_{x_2} \rangle\rangle$ , with  $\langle\langle \cdot \rangle\rangle$  denoting quantum and disorder averages, computed directly as well as its holographic estimate based on (12). We find that the behaviour for  $|x_2 - x_1| \gg 1$  and  $|x_2 - x_1| < L/2$  is indeed very similar for both approaches. We find that in the indicated distance regime, both measures of  $\langle\langle \vec{s}_{x_1} \cdot \vec{s}_{x_2} \rangle\rangle$  are consistent with the expected  $r^{-2}$  behaviour. For  $|x_2 - x_1| \gtrsim L/2$  we see that the boundaries lead to an upturn of  $\langle\langle \vec{s}_{x_1} \cdot \vec{s}_{x_2} \rangle\rangle$  for both direct and holographic estimates. This upturn is a result of boundary effects and can easily be understood in terms of the holographic TNN; for  $|x_2 - x_1| \geq L/2$ , the average path length in the tree decreases [32]. In the inset of fig. 5(a) we show the distance dependence of  $D_{\text{TTN}}$  with  $\chi = 10$ . For  $|x_2 - x_1| < L/2$ , the data can be described by as linear behaviour in  $\log|x_2 - x_1|$ . We observe that as  $L$  increases, the resulting value of the scaling power  $a$  also increases towards the expected value of 2. We have also checked that the differences between  $\chi = 10$  and 20 remain within the error bars and hence we use  $\chi = 10$  for calculations of  $\langle\langle \vec{s}_{x_1} \cdot \vec{s}_{x_2} \rangle\rangle$  in fig. 5(a). We further note that fig. 5(a) shows a clear difference in the correlation function between even and odd distances, due to the fact that singlets can only form with nearest neighbours on each coarse graining scale. While eq. (12) neatly describes the power law behaviour of the data, a more accurate ansatz should be

$$\langle\langle \vec{s}_{x_1} \cdot \vec{s}_{x_2} \rangle\rangle \simeq A \langle e^{-D_{\text{TTN}}(x_1, x_2)} \rangle^a. \quad (13)$$

We plot the fit to (13), along with the correlation data rescaled to remove the even-odd variation [33], in fig. 5(b). This shows that  $\langle\langle \vec{s}_{x_1} \cdot \vec{s}_{x_2} \rangle\rangle \approx (1.67 \pm 0.10) \langle \exp[-D_{\text{TTN}}] \rangle^{(0.69 \pm 0.01)}$  is a remarkably accurate fit to the data for all length scales. Our result implies that the majority of the correlation information is stored in the structure of the TTN rather than the contents of the tensors.

## Entanglement Entropy

In general the entanglement entropy  $S_{A|B} = -\text{Tr} \rho_A \log_2 \rho_A$  is difficult to compute as the size of the reduced density matrix  $\rho_A$  scales exponentially with the size of block A. The TTN representation of tSDRG gives an alternative means of finding  $S_{A|B}$  for any bipartitions A and B of the system. In a similar manner to the correlation functions, the geometry of the tensor network is related to its ability to capture entanglement. As discussed in the previous section,  $S_{A|B}$  is proportional to the minimum number of indices,  $n_A$ , that one would have to cut to separate a block A of spins from the rest B of the chain [16, 26]. For the TTN the position of the block in the chain alters the number of indices that have to be cut to separate it from the rest of the system. This suggests that there are spatial regions in the chain that are more and less entangled, which is likely to be true for a strongly disordered spin chain.

In refs. [35, 34], Refael and Moore calculate a *block* entanglement  $S_{A,B}$  in the random singlet phase and show that it scales as  $(\ln[2]/3) \log_2 L_B$  where region B is a block of extent  $L_B$  in the centre of the spin chain. We show the resulting  $S_{A,B}$  in fig. 6(a). The figure clearly indicates that finite size effects become prevalent for large  $L_B$ , so we fit for  $L_B \leq L/2$  only. The resulting scaling behaviour  $S_{A,B} \approx (0.22 \pm 0.02) \log_2 L_B$  is fully consistent with previous results [35]. We also examine the entanglement entropy per bond,  $S/n_A$ , of a TTN for both left-right bipartitions A|B and blocks A, B with  $\chi = 10$  when averaging over 500 disorder configurations with  $L = 50$ . Figure 6(b) shows that away from the boundaries  $S/n_A$  saturates to the same constant  $0.47 \pm 0.02$  in both cases. Note that for  $L_B \sim L/2$ , we find that up to 20% of our samples for  $\chi = 10$  lead to calculations of  $S_{A,B}$  consuming memory beyond 100GB and therefore fail to complete. Nevertheless, we believe that this will not greatly change the average values of  $S_{A,B}/n_A$  reported here as the higher failure rate is for block sizes where boundary conditions become influential, which is supported by the calculations for smaller  $\chi$ . For  $\chi = 4$  we find  $0.42 \pm 0.02$  for both blocks and bipartitions with a much lower failure rate ( $< 1\%$ ) due to the smaller size of the density matrices. This might conceivably suggest that  $S/n_A = 0.5$  is a limiting value for larger  $\chi$  and  $L$ . This is consistent with ref. [16] and implies that the entanglement entropy is proportional to the length of the holographic minimal surface that connects the two blocks.

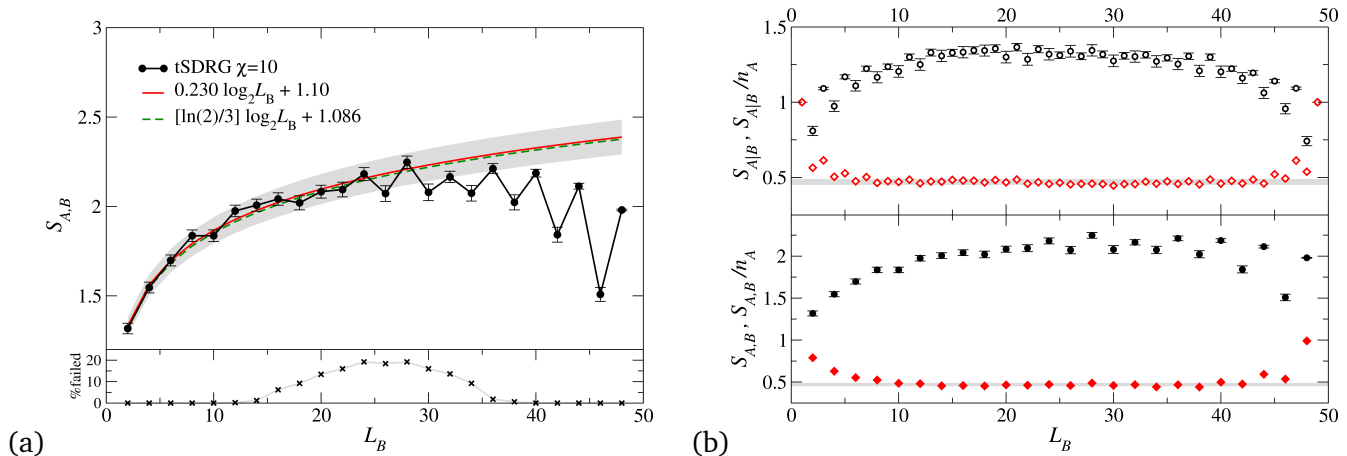


Figure 6: Reproduced from [26]. (a) The entanglement entropy  $S_{A,B}$  (black) averaged over 500 samples as a function of the size of a *block*  $L_B$  placed in the middle of a chain with  $L = 50$  for  $\chi = 10$ . The fitting (red, solid line) gives  $S_{A,B} = (0.22 \pm 0.02)\log_2 L_B + (1.12 \pm 0.05)$  for  $L_B \leq 25$ , above which finite size effects dominate. The grey shaded region indicates the accuracy of the fit. The (green) dashed line shows the entanglement scaling from ref. [34] with the vertical position fitted to the point  $L_B = 2$ . The straight black lines are a guide to the eye only. At the bottom, we show the failure rate in percent (crosses) for different  $L_B$ . (b) Entanglement entropy  $S$  (black circles) and entanglement entropy per bond  $S/n_A$  (red diamonds) for left-right bipartitions A|B (top, open symbols) and central blocks A, B (bottom, filled symbols) with  $\chi = 10$ . The entanglement per bond saturates to  $0.47 \pm 0.02$  for bipartitions and  $0.48 \pm 0.02$  for blocks (grey shaded regions).

## Conclusions and outlook

The use of tensor networks within the fields of condensed matter physics and quantum information theory is becoming ever more common. MPS based DMRG is widely believed to be the most accurate method of numerically modelling 1D systems and it is being applied in increasingly complicated scenarios [5, 4]. PEPS are being used both as a numerical method and as an analytic platform to study two dimensional strongly correlated systems, particularly topological phases of matter [36, 37]. MERA and holographic tensor networks are beginning to be applied in various other fields such as in high energy physics to potentially link entanglement and gravity [38], and quantum information in the creation of holographic error correction codes [39].

There are many ways that tensor networks can aid the study of disordered systems. Although DMRG is in some ways imperfect for the modelling of disorder, it is so efficient that much can still be learned by applying it [40]. Beyond the Heisenberg and Bose-Hubbard models, there are still a myriad of possible Hamiltonians that can be examined with DMRG. A current area of intense research is many-body localisation (MBL), the generalisation of Anderson localisation to interacting many-body systems [41]. It is believed that the area law holds for all excited states in systems with MBL up to some mobility energy, unlike gapped quantum systems where only the ground state is area law satisfying [42]. This in principle should allow for an efficient MPS representation, and therefore accurate DMRG simulation, of any state in a 1D MBL spectrum. Strong disorder renormalisation techniques such as tSDRG can be used as high precision methods when disorder is strong. The method should be accurate for use with the FM/AFM disordered spin-1/2 Heisenberg model where large effective spins would be created as the renormalisation progresses [30]. Beyond spin-1/2 there have been exciting discoveries in disordered spin-3/2 Heisenberg systems, where the rich phase diagram contains topological phases as well as spin doublet and triplet phases [43]. It would be fascinating to uncover the optimal tensor network geometries in these situations.

More generally our results suggest that it might be possible to construct an algorithm that can decide

autonomously on the best network geometry for a particular system under consideration. Currently the geometry in most tensor network approaches is set by hand using prior knowledge of the model. In a network that can self optimise the structure, the final geometry can become a resource for learning about the properties of the wavefunction. Perhaps with these ideas, truly scalable 2D and 3D tensor network algorithms may emerge for clean and disordered systems.

## References

- [1] M. Srednicki, *Phys. Rev. Lett.* **71**, 666 (1993).
- [2] M. B. Hastings, *J. Stat. Mech. Theor. Exp.* **2007**, P08024 (2007).
- [3] J. Eisert, M. Cramer, and M. B. Plenio, *Rev. Mod. Phys.* **82**, 277 (2010).
- [4] R. Orús, *Ann. Phys.* **349**, 117 (2014).
- [5] U. Schollwöck, *Ann. Phys.* **326**, 96 (2011).
- [6] J. Bekenstein, *Lett. Nuovo Cimento Series 2* **4**, 737 (1972).
- [7] S. W. Hawking, *Nature* **248**, 30 (1974).
- [8] S. Ryu and T. Takayanagi, *Phys. Rev. Lett.* **96**, 181602 (2006).
- [9] J. Maldacena, *Int. J. Theor. Phys.* **38**, 1113 (1999).
- [10] J. McGreevy, *Adv. High Energy Phys.* **2010**, 723105 (2010).
- [11] I. Peschel and V. Eisler, in *Computational Many-Particle Physics*, Vol. 739 of *Lect. Notes Phys.*, edited by H. Fehske, R. Schneider, and A. Weiß (Springer, Berlin, Heidelberg, 2008), pp. 581–596.
- [12] G. M. Crosswhite and D. Bacon, *Phys. Rev. A* **78**, 012356 (2008).
- [13] N. Laflorencie and D. Poilblanc, in *Quantum Magnetism*, edited by U. Schollwöck, J. Richter, D. J. J. Farnell, and R. F. Bishop (Springer, Berlin, Heidelberg, 2004), pp. 227–252.
- [14] K. A. Hallberg, *Adv. Phys.* **55**, 477 (2006).
- [15] S. R. White, *Phys. Rev. Lett.* **69**, 2863 (1992).
- [16] G. Evenbly and G. Vidal, *J. Stat. Phys.* **145**, 891 (2011).
- [17] G. Vidal, J. I. Latorre, E. Rico, and A. Kitaev, *Phys. Rev. Lett.* **90**, 227902 (2003).
- [18] J. I. Latorre, E. Rico, and G. Vidal, *Quantum Info. Comput.* **4**, 48 (2004).
- [19] F. Verstraete and J. I. Cirac, *arXiv:cond-mat/0407066v1* (2004).
- [20] F. Verstraete, V. Murg, and J. I. Cirac, *Adv. Phys.* **57**, 143 (2008).
- [21] G. Vidal, *Phys. Rev. Lett.* **99**, 220405 (2007).
- [22] G. Evenbly and G. Vidal, *Phys. Rev. B* **79**, 144108 (2009).
- [23] B. Swingle, *Phys. Rev. D* **86**, 065007 (2012).
- [24] M. Nozaki, S. Ryu, and T. Takayanagi, *J. High Energy Phys.* **2012**, 193 (2012).

- [25] A. Mollabashi, M. Nozaki, S. Ryu, and T. Takayanagi, *J. High Energy Phys.* **2014**, 1 (2014).
- [26] A. M. Goldsborough and R. A. Römer, *Phys. Rev. B* **89**, 214203 (2014).
- [27] S.-k. Ma, C. Dasgupta, and C.-k. Hu, *Phys. Rev. Lett.* **43**, 1434 (1979).
- [28] C. Dasgupta and S.-k. Ma, *Phys. Rev. B* **22**, 1305 (1980).
- [29] D. S. Fisher, *Phys. Rev. B* **50**, 3799 (1994).
- [30] T. Hikihara, A. Furusaki, and M. Sigrist, *Phys. Rev. B* **60**, 12116 (1999).
- [31] K. G. Wilson, *Rev. Mod. Phys* **47**, 773 (1975).
- [32] A. M. Goldsborough *et al.*, arXiv:1502.07893 [math-ph] (2015).
- [33] J. A. Hoyos, A. P. Vieira, N. Laflorencie, and E. Miranda, *Phys. Rev. B* **76**, 174425 (2007).
- [34] G. Refael and J. E. Moore, *Phys. Rev. B* **76**, 024419 (2007).
- [35] G. Refael and J. E. Moore, *Phys. Rev. Lett.* **93**, 260602 (2004).
- [36] T. B. Wahl, H.-H. Tu, N. Schuch, and J. I. Cirac, *Phys. Rev. Lett.* **111**, 236805 (2013).
- [37] D. Poilblanc, J. I. Cirac, and N. Schuch, *Phys. Rev. B* **91**, 224431 (2015).
- [38] B. Swingle and M. V. Raamsdonk, arXiv:1405.2933 [hep-th] (2014).
- [39] F. Pastawski, B. Yoshida, D. Harlow, and J. Preskill, *J. High Energy Phys.* **2015**, 1 (2015).
- [40] A. M. Goldsborough and R. A. Römer, *EPL* **111**, 26004 (2015).
- [41] D. Basko, I. Aleiner, and B. Altshuler, *Ann. Phys.* **321**, 1126 (2006).
- [42] A. Chandran *et al.*, *Phys. Rev. B* **92**, 024201 (2015).
- [43] V. L. Quito, J. A. Hoyos, and E. Miranda, *Phys. Rev. Lett.* **115**, 167201 (2015).

# Hydrogen and helium under extreme pressures

Bartomeu Monserrat

## Introduction

Hydrogen and helium account for almost all the visible matter in the Universe, with hydrogen representing 75% of the total, and helium the rest. As a consequence, they are major components of all astrophysical objects, from giant planets, to stars and white dwarf stars. Inside these celestial bodies, they are found under extreme conditions of temperature and pressure, unattainable in the laboratory. For example, hydrogen is thought to be present in the core of Jupiter, where the pressure reaches several terapascal; this is 10 times larger than the pressure at the core of the Earth, and over 10 million times larger than atmospheric pressure.

Computational methods for the description of the quantum mechanics of electrons and nuclei allow us to study these systems under the relevant conditions in a computer. Electrons play a central role in the properties of matter, from structure to electronic, optical, magnetic, and thermal behaviour. Computational methods such as density functional theory (DFT) and quantum Monte Carlo (QMC) allow us to describe the electronic structure of matter with high accuracy. The heavier atomic nuclei can often be treated as a static background to the electrons. However, for the light elements – hydrogen and helium being the lightest of all – and at high temperature, nuclear motion becomes central, and a proper quantum description is required.

Here, we will describe the theoretical and computational methods proposed in the thesis to accurately describe the quantum mechanical motion of atomic nuclei, and their application to the study of the phase diagrams of hydrogen and helium at high pressure. In particular, new methods to describe anharmonic vibrations in solids composed of light elements, and the coupling of nuclear motion to electrons will prove essential for a correct understanding of the physics of these systems. In Sec. , we will describe the first theoretical study of hydrogen in the pressure range 100–400 GPa that allows us to explain the existence of a temperature-stabilised structure known as phase IV. In Sec. , we will study the metallisation of solid helium, which is found to occur at about 30 TPa, and which has major implications for the cooling of white dwarfs and the field of cosmochemistry.

## Phase diagrams

The computational construction of phase diagrams involves two steps:

1. The search for candidate structures under the conditions of interest.
2. The accurate calculation of their Gibbs free energy, in order to determine the thermodynamically stable structures.

Computational studies start by identifying a range of candidate structures using structure searching methods. In the case of hydrogen, the seminal works of Pickard and Needs [1, 2] using the *ab initio* random structure searching (AIRSS) method [3, 4] provided many of the structures that are energetically competitive in the pressure range 100–400 GPa. AIRSS works on a very simple but effective principle: select a set of random positions for the atoms in a random simulation cell, and then relax the initial structure to the local minimum of enthalpy. Repeating this process a large number of times provides a fair description of configuration space, and delivers a range of candidate structures. The basic AIRSS algorithm can be modified by the application of constraints, such as symmetry or minimum atomic distances.

In this work, our focus will be on the second step of the construction of phase diagrams. The Gibbs free energy  $\mathcal{G}$  of a solid at pressure  $P$  and temperature  $T$  is:

$$\mathcal{G} = \mathcal{F}_n + \mathcal{F}_e, \quad (14)$$

where the Helmholtz free energy is given by  $\mathcal{F} = E - TS$  for energy  $E$  and entropy  $S$ . The phase diagram is constructed with the structures that minimise the Gibbs free energy.

The electronic component of the Gibbs free energy is typically calculated using density functional theory or, if a higher degree of accuracy is required, diffusion Monte Carlo. These are both well established methods. The nuclear motion component of the Gibbs free energy is usually calculated using the harmonic approximation. Within this approximation, nuclear vibrations of small amplitude about equilibrium are considered, and the resulting Hamiltonian reads:

$$\mathcal{H}_{\text{har}} = \sum_{\mathbf{q}, \nu} -\frac{1}{2} \frac{\partial^2}{\partial u_{\mathbf{q}\nu}^2} + \frac{1}{2} \omega_{\mathbf{q}\nu}^2 u_{\mathbf{q}\nu}^2, \quad (15)$$

where  $u_{\mathbf{q}\nu}$  is the amplitude of a normal mode coordinate labelled by wavevector  $\mathbf{q}$  and branch index  $\nu$ , and  $\omega_{\mathbf{q}\nu}$  is the corresponding frequency. Equation (15) is particularly suitable for computation, as each degree of freedom is decoupled from others, and in practice one only has a large number of 1-dimensional equations. In fact, the Schrödinger equation resulting from the harmonic approximation can be solved analytically.

For light elements such as hydrogen or helium, the assumption that nuclear vibrations have small amplitudes is no longer valid, and potential energy terms beyond the quadratic term in Eq. (15) need to be considered. These are called *anharmonic* terms. To retain the computational simplicity of the harmonic approximation, we choose to represent the anharmonic potential energy by the principal axes approximation [5]:

$$\mathcal{H}_{\text{anh}} = \sum_{\mathbf{q}, \nu} -\frac{1}{2} \frac{\partial^2}{\partial u_{\mathbf{q}\nu}^2} + \sum_{\mathbf{q}, \nu} V_{\mathbf{q}\nu}(u_{\mathbf{q}\nu}) + \frac{1}{2} \sum_{\mathbf{q}, \nu} \sum'_{\mathbf{q}', \nu'} V_{\mathbf{q}\nu; \mathbf{q}'\nu'}(u_{\mathbf{q}\nu}, u_{\mathbf{q}'\nu'}) + \dots, \quad (16)$$

where the prime sum indicates that the term  $(\mathbf{q}, \nu) = (\mathbf{q}', \nu')$  is excluded, and the factor 1/2 accounts for double counting. Note that the harmonic approximation is recovered for  $V_{\mathbf{q}\nu}(u_{\mathbf{q}\nu}) = \frac{1}{2} \omega_{\mathbf{q}\nu}^2 u_{\mathbf{q}\nu}^2$ , and setting all other terms to zero. Otherwise, an anharmonic potential energy is obtained.

The anharmonic potential energy in Eq. (16) has the advantage that the one-body term, which typically dominates, is still a set of one-dimensional uncoupled terms, the same computational complexity as the harmonic approximation. Higher-order terms leads to increasing complexity, and a balance between accuracy and computational expense needs to be considered. The anharmonic Schrödinger equation no longer has analytic solutions, and instead we solve it using a mean-field approach for the anharmonic vibrational wave function  $|\Phi\rangle = \prod_{\mathbf{q}, \nu} |\phi_{\mathbf{q}\nu}(u_{\mathbf{q}\nu})\rangle$ ,

$$\mathcal{H}_{\text{anh}}|\Phi\rangle = E_{\text{anh}}|\Phi\rangle. \quad (17)$$

The anharmonic vibrational nuclear energy  $E_{\text{anh}}$  is obtained by minimising the energy with respect to the single-particle states  $|\phi_{\mathbf{q}\nu}\rangle$ .

The wave function of any quantum system contains all the information about the state of the system. Therefore, once the anharmonic vibrational equations have been solved to determine the vibrational nuclear energy and wave function, expectation values of other physical properties may be calculated. For a quantity with observable  $\hat{O}$ , the expectation at temperature  $T$  is:

$$\langle \hat{O} \rangle = \frac{1}{\mathcal{Z}} \sum_{\mathbf{M}} \langle \Phi_{\mathbf{M}} | \hat{O} | \Phi_{\mathbf{M}} \rangle e^{-E_{\mathbf{M}}/k_{\text{B}}T}, \quad (18)$$

where  $\mathcal{Z} = \sum_{\mathbf{M}} e^{-E_{\mathbf{M}}/k_{\text{B}}T}$  is the partition function,  $\mathbf{M}$  represents a quantum state, and  $k_{\text{B}}$  is Boltzmann's constant. Equation (18) may be evaluated by a many-body expansion parallel to the energy expansion in Eq. (16), or alternatively by using Monte Carlo sampling over the vibrational density. As an example, if the quantity of interest is the electronic band gap, then the expectation value in Eq. (18) may be used to calculate the temperature dependence of the band gap due to electron-phonon coupling.

With the treatment of nuclear vibrations described above, we are now equipped to study the phase diagrams of hydrogen and helium under extreme pressures. All density functional theory calculations have

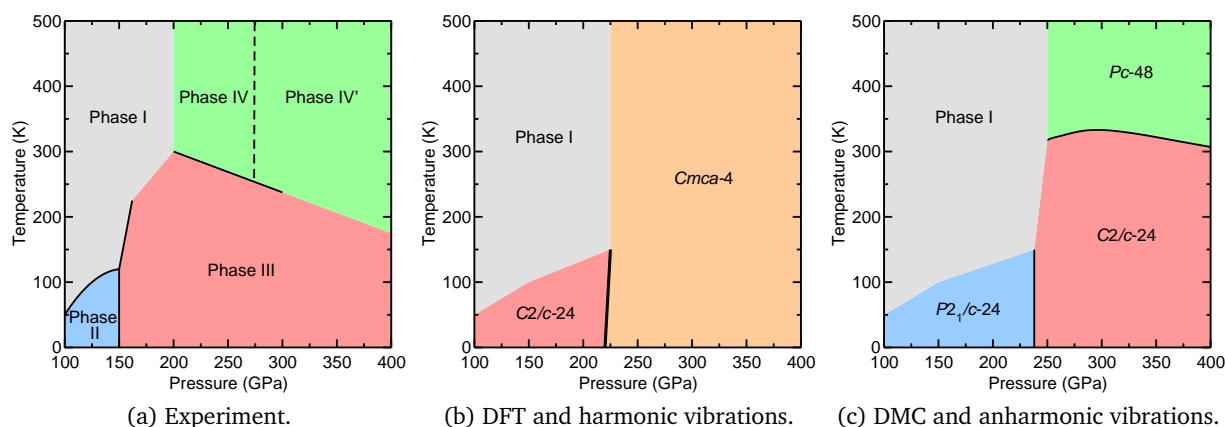


Figure 1: Phase diagram of high pressure hydrogen determined experimentally (left), computationally using DFT and the harmonic approximation (center), and computationally using DMC and including anharmonic vibrations (right).

been performed using the plane-wave pseudopotential code CASTEP [6], and numerical details of the calculations are provided in the corresponding references. The quantum Monte Carlo calculations, performed by collaborators, have used the CASINO program [7].

## High pressure hydrogen

Hydrogen is the simplest of all elements – a proton and an electron – but its phase diagram is rich and challenging to study. Static high pressure experiments have reached pressures just above those at the centre of the Earth, of up to 400 GPa. Raman and infrared (IR) spectroscopies have been used to probe these high pressure systems, establishing the existence of at least four high pressure solid phases of hydrogen, as shown in Fig. 1a. Phase IV, which appears to be stable only above room temperature at the higher pressure range, was only discovered recently [8, 9]. Protons scatter X-rays very weakly, and Raman and IR data are insufficient to unambiguously identify the crystal structures of the observed phases.

Candidate structures for the high pressure phases of hydrogen were identified in the seminal works of Pickard and Needs using the AIRSS method. However, the standard calculations of the relative Gibbs free energies of these structures, using DFT for the electronic energy and the harmonic approximation for the vibrational energy, fail to reproduce the experimental phase diagram, as shown in Fig. 1b. In particular, there appears to be no structure corresponding to phase IV.

This thesis shows that the more accurate diffusion Monte Carlo method for the calculation of the electronic energy, together with the inclusion of anharmonic nuclear motion, are required to predict a phase diagram with boundaries in qualitative agreement with experiment, shown in Fig. 1c. The use of state of the art quantum mechanical methods for the description of both electrons and nuclei allows us to accurately reproduce the known phases of high pressure hydrogen. It is then possible to go beyond those pressures accessible in the laboratory, and study the metallisation and dissociation of hydrogen [10], pushing our models closer to the pressures found at the interiors of giant planets and stars.

## High pressure helium

The two electrons in the helium atom fill the  $1s$  state, rendering helium an inert noble gas. Under pressure, the electronic distribution in a material delocalises, and at sufficiently high pressures all materials are metallic. The inertness of helium atoms leads to extraordinarily high pressures for the metallisation of the solid phase, only accomplished in the terapascal pressure range. Helium under these pressures is a major

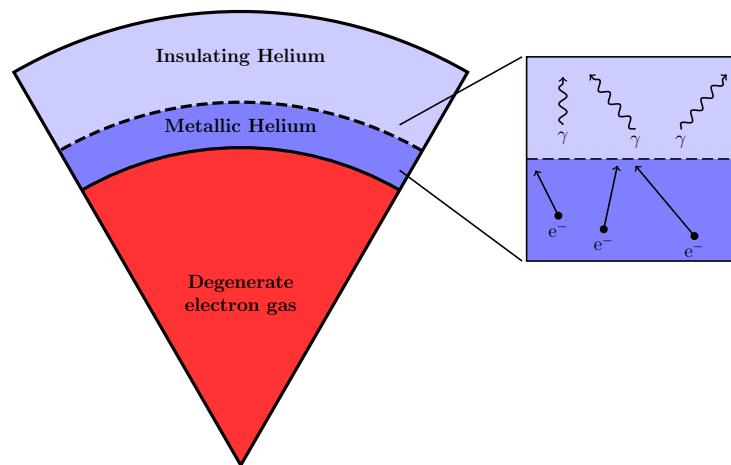


Figure 2: Cross section showing the interior of a white dwarf star. The core (red) is dominated by the electron degenerate matter and is isothermal. The helium-dominated outer layers are metallic at higher pressures (dark blue), and insulating closer to the surface (light blue). Electrons carry heat through metallic helium, but slower photon diffusion dominates in the insulating layer.

component of the outer layers of white dwarfs, and as such plays a major role in the cooling rate of these stars.

White dwarf stars constitute the final stage in the life of the vast majority of stars in the Universe, and our own Sun will become a white dwarf in a few billion years. The nuclear fuel in the interior of these stars has been exhausted, and their immense gravitational pull has contracted them to very high densities. At sufficiently high densities, the electrons are pushed close together, and the Pauli exclusion principle that prevents any two electrons from occupying the same state leads to the so-called electronic pressure, that for white dwarfs is sufficient to balance the gravitational pull inwards. Thus, white dwarfs, although initially hot, do not have an internal energy source, and therefore cool down over timescales of billions of years to reach thermodynamic equilibrium with the surrounding cold Universe. The cooling rate is initially very high, but it decreases dramatically below about 10,000 K. In fact, it becomes so slow that it is believed the Universe is not old enough for any white dwarf star to have cooled to 2.7 K yet, the temperature of the cosmic microwave background.

Understanding the cooling rate of white dwarfs, together with observations of their current temperatures – that are related to their luminosity – allows astrophysicists to date these stars. From these dates, lower limits may be placed on the ages of stellar clusters, galaxies, and indeed the entire Universe. This is the field of chosmochronology – the dating of the cosmos. Crucially, accurate dates can only be achieved if the cooling rate of white dwarfs is fully understood, which requires an understanding of the rate of heat transport from the hot isothermal core, through the outer layers, and to the surface. The helium-rich outer layers make an understanding of the phase diagram of helium central to this problem.

In Fig. 2 we show a schematic cross-section of a white dwarf. The large core (in red) is composed of the degenerate electrons that balance the gravitational pull, and is isothermal. The helium-rich outer layers can be separated into the metallic helium inner layer (dark blue) at higher pressure, and the insulating helium outer layer (light blue). Heat is carried by mobile electrons through the metal, but upon reaching the insulating layer, the much slower photon diffusion is the dominant mechanism. An understanding of the metallisation conditions of helium therefore has profound consequences for the relative importance of the two layers, and for the overall cooling rate of white dwarfs.

Early estimates of the metallisation of helium were based on the calculation of the closing of the electronic band gap as a function of pressure. These calculations, performed using the diffusion Monte Carlo method, neglected the influence of nuclear motion on the electrons. The most accurate calculations predicted a metallisation pressure of 27 TPa [13]. In this thesis, we included the coupling of electrons to nuclear



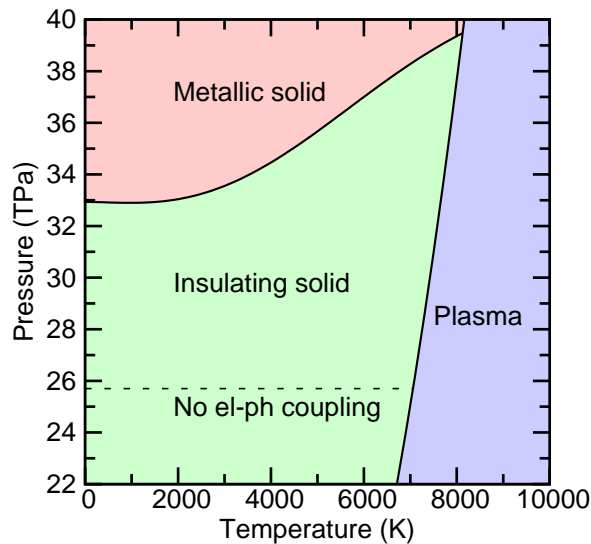


Figure 3: Phase diagram of helium at high pressure. The new metal-insulator boundary captures the temperature dependence with the inclusion of electron-phonon coupling. The transition to the plasma phase is taken from Ref. [11]. This diagram is reproduced from Ref. [12]

vibrations (so-called electron-phonon coupling), to predict a new higher metallisation pressure for helium, of 32 TPa at zero temperature. Furthermore, as nuclear motion encapsulates the changes in matter due to temperature, our predictions could be extended to finite temperatures, as shown in the phase diagram of Fig. 3.

The higher metallisation pressure that we predict for solid helium implies that the outer insulating layers in white dwarfs are wider than previously believed. Therefore, the cooling rate of white dwarf stars is slower, and this calls for a revision of current estimates of the ages of these stars.

## Outlook

The new theoretical and computational methods proposed in the thesis, and described in this work, have allowed us to calculate the phase diagrams of high pressure solid hydrogen and helium with unprecedented accuracy. These new phase diagrams are essential for the description of the physical processes found in astrophysical objects, such as the strong magnetic fields around giant planets, or the cooling rate of white dwarf stars.

Increasing computational power, together with new methods and algorithmic improvements, continue to expand the pressure-temperature regimes of physics that can be explored. The methods described in this thesis could find ample application for the study of other high-pressure compounds, for example those found in the interior of the Earth, whose chemistry adds a new layer of complexity. Furthermore, the methods presented here are not limited to the study of high pressure. Temperature is important in many interesting physical processes, and the accurate description of quantum nuclear motion becomes central. Indeed, we have successfully applied the methods described here to address problems in a wide range of areas, from explaining why snowflakes are hexagonal rather than cubic [14], to understanding the effects of temperature on nuclear magnetic resonance spectra [15]. Continued development of new algorithms has significantly reduced the computational cost of the methods first proposed in the thesis [16, 17], paving the way for new and complex applications.

## Acknowledgments

The work described here as part of the PhD thesis has been performed under the supervision of Prof. Richard J. Needs, whose advice is gratefully acknowledged. Prof. Chris J. Pickard, Dr Neil Drummond, Dr Pablo López Ríos, and Dr Jonathan H. Lloyd-Williams have been close collaborators.

## References

- [1] Chris J. Pickard and Richard J. Needs. Structure of phase III of solid hydrogen. *Nat. Phys.*, 3(7):473–476, Jul 2007.
- [2] Chris J. Pickard, Miguel Martinez-Canales, and Richard J. Needs. Density functional theory study of phase IV of solid hydrogen. *Phys. Rev. B*, 85:214114, Jun 2012.
- [3] Chris J. Pickard and R. J. Needs. High-pressure phases of silane. *Phys. Rev. Lett.*, 97:045504, Jul 2006.
- [4] Chris J. Pickard and R. J. Needs. *Ab initio* random structure searching. *J. Phys. Condens. Matter*, 23(5):053201, 2011.
- [5] Bartomeu Monserrat, N. D. Drummond, and R. J. Needs. Anharmonic vibrational properties in periodic systems: Energy, electron-phonon coupling, and stress. *Phys. Rev. B*, 87:144302, Apr 2013.
- [6] Stewart J. Clark, Matthew D. Segall, Chris J. Pickard, Phil J. Hasnip, Matt I. J. Probert, Keith Refson, and Mike C. Payne. First principles methods using CASTEP. *Z. Kristallogr.*, 220:567, 2005.
- [7] R. J. Needs, M. D. Towler, N. D. Drummond, and P. López Ríos. Continuum variational and diffusion quantum Monte Carlo calculations. *J. Phys. Condens. Matter*, 22(2):023201, 2010.
- [8] M. I. Eremets and I. A. Troyan. Conductive dense hydrogen. *Nat. Mater.*, 10:927, 2011.
- [9] Ross T. Howie, Christophe L. Guillaume, Thomas Scheler, Alexander F. Goncharov, and Eugene Gregoryanz. Mixed molecular and atomic phase of dense hydrogen. *Phys. Rev. Lett.*, 108:125501, Mar 2012.
- [10] Sam Azadi, Bartomeu Monserrat, W. M. C. Foulkes, and R. J. Needs. Dissociation of high-pressure solid molecular hydrogen: A quantum Monte Carlo and anharmonic vibrational study. *Phys. Rev. Lett.*, 112:165501, Apr 2014.
- [11] Andreas Förster, Torsten Kahlbaum, and Werner Ebeling. Equation of state and the phase diagram of dense fluid helium in the region of partial ionization. *Laser Part. Beams*, 10:253–262, 5 1992.
- [12] Bartomeu Monserrat, N. D. Drummond, Chris J. Pickard, and R. J. Needs. Electron-phonon coupling and the metallization of solid helium at terapascal pressures. *Phys. Rev. Lett.*, 112:055504, Feb 2014.
- [13] S. A. Khairallah and B. Militzer. First-principles studies of the metallization and the equation of state of solid helium. *Phys. Rev. Lett.*, 101:106407, Sep 2008.
- [14] Edgar A. Engel, Bartomeu Monserrat, and Richard J. Needs. Anharmonic nuclear motion and the relative stability of hexagonal and cubic ice. *Phys. Rev. X*, 5:021033, Jun 2015.
- [15] Bartomeu Monserrat, Richard J. Needs, and Chris J. Pickard. Temperature effects in first-principles solid state calculations of the chemical shielding tensor made simple. *J. Chem. Phys.*, 141(13):134113, 2014.

- [16] Jonathan H. Lloyd-Williams and Bartomeu Monserrat. Lattice dynamics and electron-phonon coupling calculations using nondiagonal supercells. *Phys. Rev. B*, 92:184301, Nov 2015.
- [17] Bartomeu Monserrat. Vibrational averages along thermal lines. *Phys. Rev. B*, 93:014302, Jan 2016.

# Computational Physics Group News

## • The Computational Physics Annual PhD Thesis Prize

Each year, the IoP Computational Physics Group awards a Thesis Prize to the author of the PhD thesis that, in the opinion of the Committee, contributes most strongly to the advancement of computational physics.

The winner of the 2016 Thesis Prize is Cathal Ó Broin for his thesis entitled *A New GPU-based Computational Framework for the Ab-initio Solution of the TDSE for Atomic and Molecular One-Electron Systems under Intense Ultra-Short Laser Fields*, which was undertaken at Dublin City University.

Runner-up prizes 2016 are awarded to Andrew Goldsborough, for his thesis entitled *Tensor Networks and Geometry for the Modelling of Disordered Quantum Many-Body Systems*, carried out at the University of Warwick, and Patrick Cannon, for his thesis entitled *Numerical Simulation of Wave-Plasma Interactions in the Ionosphere*, carried out at the University of Lancaster.

Thanks to the generosity of AWE ([www.awe.co.uk](http://www.awe.co.uk)) Cathal receives £300 and Andrew and Patrick receive £100 each for their achievements. Articles describing Cathal and Andrew's work appear earlier in this issue, together with the work of Bartomeau Monserrat who was a runner-up in last year's competition.

Details of Patrick's work will appear in a forthcoming issue of the newsletter.

For this year's prize applications are encouraged across the entire spectrum of computational physics. Entry is open to all students from an institution in the UK or Ireland, whose PhD examination has taken place since 1st January 2016 and up to the submission deadline.

Prize winners will be invited to write a feature article in the Computational Physics Group newsletter. The submission deadline is **30 April 2017**.

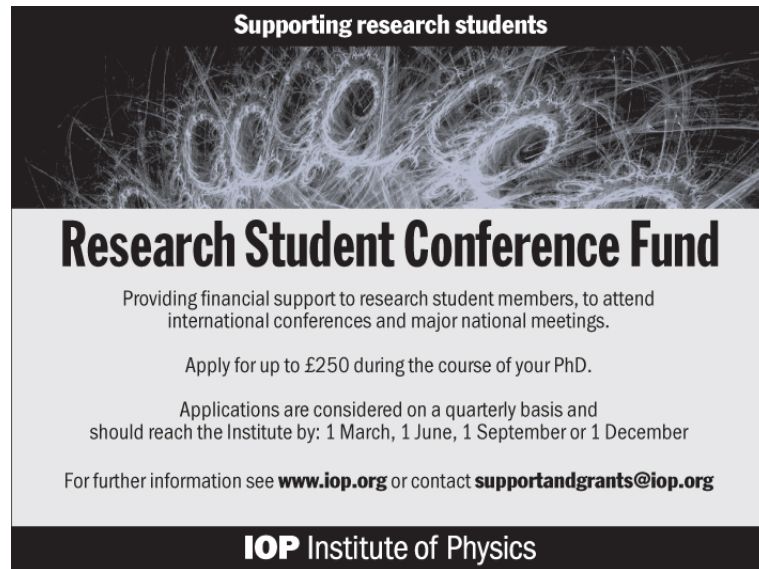
Candidates are asked to note that a similar thesis prize is offered by the Theory of Condensed Matter (Computational Physics) Group and the Committees have agreed that both prizes will not be awarded to the same applicant.

The submission format is as follows:

- A four page (A4) abstract describing the background and main achievements of the work
- A one page (A4) citation from the PhD supervisor
- A one page (A4) confidential report from the external thesis examiner

Entries (PDF documents preferred) should be submitted by email, with "IOP CPG Thesis Prize" as the subject header, to Dr Arash Mostofi ([a.mostofi@imperial.ac.uk](mailto:a.mostofi@imperial.ac.uk)). Any queries should also be directed to Dr Arash Mostofi. A few more details, including a list of past winners, can be found on the group webpage [http://www.iop.org/activity/groups/subject/comp/prize/page\\_40691.html](http://www.iop.org/activity/groups/subject/comp/prize/page_40691.html).

## • IoP Computational Physics Group - Research Student Conference Fund



Supporting research students

### Research Student Conference Fund

Providing financial support to research student members, to attend international conferences and major national meetings.

Apply for up to £250 during the course of your PhD.

Applications are considered on a quarterly basis and should reach the Institute by: 1 March, 1 June, 1 September or 1 December

For further information see [www.iop.org](http://www.iop.org) or contact [supportandgrants@iop.org](mailto:supportandgrants@iop.org)

**IOP** Institute of Physics

The Institute of Physics Computational Physics Group is pleased to invite requests for partial financial support towards the cost of attending scientific meetings relevant to the Group's scope of activity. The aim of the scheme is to help stimulate the career development of young scientists working in computational physics to become future leaders in the field.

Further details on this award can be found at:

[www.iop.org/about/grants/research\\_student/page\\_38808.html](http://www.iop.org/about/grants/research_student/page_38808.html)

## Conference and Workshop reports

### • 47<sup>th</sup> Annual APS-DAMOP Meeting Providence (RI), USA, 2016.

23-27 May 2015 at Rhoda Island, USA.

**Highlights.** The regular DAMOP Meeting is an annual conference organised by the Division of Atomic and Molecular Optics of the American Physical Society. This year's edition has been held in Providence (Rhode Island) in the United States, in the period between the 23rd and the 27th day of May. It is usually a very large event: the number of participants was of the order of 2000, with 92 invited speakers and hundreds of contributed talks. The participants include some of the most prominent researchers in atomic and optical physics. This edition comprehended people from the best experimental and theoretical groups in the world (MIT, Harvard, JILA, JQI, Rice, LENS, Trento, Cambridge, Munich, ENS, among the others), often including the principal investigators. It has also been an extraordinary chance for PhD students and young researchers to grasp a broader spectrum of the activities related to the field of Bose-Einstein Condensates, and to present their work to a vast and outstanding audience. The conference was structured as follows: Monday 23rd a Graduate Student Symposium was held, mainly devoted to postgraduate students, including four introductory lectures on different hot topics in the field of BEC; from Tuesday 24th to Friday 27th, a large number of invited and contributed talk sessions on various categories of research activities were organised. There were up to 8 parallel talk sessions, and the people were free to move from one to another, so to follow the most interesting seminars. Moreover, three different poster sessions were set up, each showing more than hundred posters. **Benefits.** I had the great opportunity to talk to many researchers about my and their

research, and to share ideas and impressions about the direction towards which I should point. In particular, thanks to the fact that I had a contributed talk slot, I could present my results to a large audience, and collect comments and suggestions about them. Moreover, I had the opportunity to meet with both my supervisors (prof. Franco Dalfovo (Trento) and prof. Nick Proukakis (Newcastle)), and we had deep and valuable discussions about our common work. Aside from the conference, I visited the BEC experimental laboratories at MIT and I was introduced to the research activities performed therein. **Success.** I truly believe the conference was fully successful, and indeed it was reported to be the most participated ever organised DAMOP meeting. I consider this kind of meeting to be of great importance for the advancement of science, and I hope to be able to participate again.

*Report kindly provided by Fabrizio Larcer, PhD student, JQC Durham-Newcastle and University of Trento*

## • American Physical Society (APS), USA, 2016.

14-18 March 2016 Baltimore, USA.

The APS March Meeting is an annual conference organised by the American Physical Society, it gathers physicists from many different areas to share groundbreaking research from industry, universities, and major laboratories. This year's March Meeting was held at the convention centre in Baltimore, which is located in the downtown area of Baltimore and just a five minute walk from the Inner Harbour area. Almost 10,000 people were in attendance, with around 9,000 people giving talks over 5 days (myself included). There were 24 APS units represented at the conference including the Atomic, Molecular & Optical Physics division, Materials Physics division, the Quantum Information Topical group, the Industrial & Applied Physics forum, and many more. The days were split up into three sessions, with each session being around two and a half hours. Most talks contained within these session were ten minutes with two minutes for questions, though sometimes there would be invited talks from some of the big groups which would be half an hour. As my research area is in superconducting circuits this is where I spent most of my time. This conference is a very important one as it gives everyone the opportunity to find out about work being performed by research groups around the world, and to publicise your own work with the potential for feedback and collaboration with other groups if they find interest in your work. Generally much of the work that was presented had not yet been published, so attending the conference was a great way to find out about research groups results ahead of publication and to look out for potential publications in the near future. In particular it was great to listen to the talks coming from the big research groups in superconducting circuits such as Yale, Google, and IBM. The advances that these groups have made towards building quantum computers in the past year have been astounding and the results produced at the meeting this year have shown how much further we have come towards this goal. Apart from the focus sessions there were also invited sessions which would give an overview of a specific area, with the talks being given by some of the big names within that research area. On the Wednesday there was an invited session titled 20 Years of Quantum Error Correction with talks being given by people such as John Preskill, Daniel Gottesman, David DiVincenzo, Philipp Schindler and Michel Devoret. It was great to see talks given by some of the people who had effectively started the field and made for great listening. These invited session were also a great opportunity to listen to talks that may not be in your field as they were more accessible than the focus talks. For example, I attended a session on Physics and Cancer which was a very interesting set of talks on how physics could be used in the "war on cancer". In all the conference was a great one to attend - it gave me the opportunity to present my work to groups who may not necessarily have seen it otherwise, and to obtain feedback from my peers. I was able to see the most recent results produced by research groups before the official publication and was provided with the opportunity to directly interact with researchers from these groups and to ask questions on their work.

## Upcoming Events of Interest

Upcoming events of interest to our readers can now be found via the following web links.

- IOP's index page for scientific meetings, including conferences, group events and international workshops:  
[www.iop.org/events/scientific/index.html](http://www.iop.org/events/scientific/index.html)
- IOP Conferences page for conference information, calendar and noticeboard:  
[www.iop.org/events/scientific/conferences/index.html](http://www.iop.org/events/scientific/conferences/index.html)
- All events being run or supported by IOP Groups including calendar and links to event web pages:  
[www.iop.org/events/scientific/group/index.html](http://www.iop.org/events/scientific/group/index.html)
- Thomas Young Centre: The London Centre for Theory and Simulation of Materials organises many different kinds of scientific events on the theory and simulation of materials, including Highlight Seminars, Soirees and Workshops. For further details of upcoming events please visit:  
[www.thomasyoungcentre.org/events/](http://www.thomasyoungcentre.org/events/)
- CECAM is a European organization devoted to the promotion of fundamental research on advanced computational methods for atomistic and molecular simulation and their application to important problems in science and technology. CECAM organises a series of scientific workshops, tutorials and meetings. For further details please visit:  
[www.cecaml.org](http://www.cecaml.org)

## Computational Physics Group Committee

The current members of the IoP Computational Physics Group committee with their contact details are as follows:

Hans Fangohr	<a href="mailto:h.fangohr@soton.ac.uk">h.fangohr@soton.ac.uk</a>
Vera Hazelwood (Chair)	<a href="mailto:Vera.Hazelwood@smithinst.co.uk">Vera.Hazelwood@smithinst.co.uk</a>
Stephen Hughes	<a href="mailto:Stephen.Hughes@awe.co.uk">Stephen.Hughes@awe.co.uk</a>
Paul Hulse	<a href="mailto:paul.hulse@sellafieldsites.com">paul.hulse@sellafieldsites.com</a>
Arash Mostofi (Thesis prize)	<a href="mailto:a.mostofi@imperial.ac.uk">a.mostofi@imperial.ac.uk</a>
John Pelan	<a href="mailto:j.pelan@gatsby.ucl.ac.uk">j.pelan@gatsby.ucl.ac.uk</a>
Marco Pinna (Newsletter)	<a href="mailto:mpinna@lincoln.ac.uk">mpinna@lincoln.ac.uk</a>
David Quigley	<a href="mailto:d.quigley@warwick.ac.uk">d.quigley@warwick.ac.uk</a>
Simon Richards	<a href="mailto:s.richards@physics.org">s.richards@physics.org</a>
Jesus Rogel (Secretary)	<a href="mailto:j.rogel@physics.org">j.rogel@physics.org</a>
David Shipley	<a href="mailto:david.shipley@npl.co.uk">david.shipley@npl.co.uk</a>
Nathan Sircombe (Treasurer)	<a href="mailto:Nathan.Sircombe@awe.co.uk">Nathan.Sircombe@awe.co.uk</a>
Nick Parker	<a href="mailto:nick.parker@ncl.ac.uk">nick.parker@ncl.ac.uk</a>

Some useful web links related to the Computational Physics Group are:

- CPG webpages  
[comp.iop.org](http://comp.iop.org)
- CPG Newsletters  
Current issue:  
[www.iop.org/activity/groups/subject/comp/news/page\\_40572.html](http://www.iop.org/activity/groups/subject/comp/news/page_40572.html)  
Previous issues:  
[www.iop.org/activity/groups/subject/comp/news/archive/page\\_53142.html](http://www.iop.org/activity/groups/subject/comp/news/archive/page_53142.html)  
[www.soton.ac.uk/~fangohr/iop\\_cpg.html](http://www.soton.ac.uk/~fangohr/iop_cpg.html)

## Related Newsletters and Useful Websites

The Computational Physics Group works together with other UK and overseas computational physics groups. We list their newsletter locations and other useful websites here:

- Newsletter of the Computational Physics Division of the American Physical Society:  
[www.aps.org/units/dcomp/newsletters/index.cfm](http://www.aps.org/units/dcomp/newsletters/index.cfm)
- Europhysicsnews newsletter of the European Physical Society (EPS):  
[www.europhysicsnews.org/](http://www.europhysicsnews.org/)
- Newsletter of the Psi-k ( $\Psi_k$ ) network:  
[www.psi-k.org/newsletters.shtml](http://www.psi-k.org/newsletters.shtml)